Chemical Engineering Science 127 (2015) 293–309

Contents lists available at ScienceDirect

Chemical Engineering Science

journal homepage: www.elsevier.com/locate/ces

Direct perturbation of the Peng–Robinson attraction and covolume parameters for reservoir fluid characterization

Ashutosh Kumar, Ryosuke Okuno *

School of Mining and Petroleum Engineering, University of Alberta, Edmonton, AB, Canada

HIGHLIGHTS

- A new method is presented for reservoir fluid characterization.
- The Peng–Robinson equation of state is used with the van der Waals mixing rules.
- The attraction and covolume parameters of pseudo components are directly adjusted.
- Apparent critical parameters of pseudo components are not needed.
- The method is tested for characterization of 84 different reservoir fluids.

ARTICLE INFO

Article history:
Received 4 June 2014
Received in revised form
3 December 2014
Accepted 16 January 2015
Available online 28 January 2015

Keywords:
Equations of state
Fluid characterization
Petroleum reservoir fluids
Attraction and covolume parameters
Perturbation from *n*-alkanes

ABSTRACT

Numerical simulation of enhanced oil recovery processes, such as gas and steam floods, requires that the reservoir fluid of interest is reliably modeled by use of an equation of state (EOS). Reservoir fluid characterization using an EOS can be challenging because of the uncertainties associated with non-identifiable heavy fractions, which are characterized as a few pseudo components.

This paper presents a new method for reservoir fluid characterization that directly perturbs the attraction and covolume parameters of pseudo components from the *n*-alkanes' values (direct perturbation from *n*-alkanes, or direct PnA). The direct PnA method systematically adjusts the attraction and covolume parameters of all pseudo components within a given reservoir fluid through a few adjustable parameters. As in our prior research, the $\psi(=a/b^2)$ parameter is used to ensure the proper interrelationship between the attraction (a) and covolume (b) parameters. A new approach to adjustment of the ψ parameters is developed with a linear relationship of ψ with molecular weight. The Peng–Robinson (PR) EOS is used throughout the research.

The direct PnA method is applied to 84 different reservoir fluids, such as gas condensates, volatile oils, and heavy oils. Characterization of each fluid uses the saturation pressure and liquid density data at different pressures at the reservoir temperature. Other phase behavior data available are used to test the predictive capability of the fluid models developed using the PR EOS with the direct PnA method. Results show that the reservoir fluids tested are reliably characterized by the systematic control over phase behavior predictions in the direct PnA method. Unlike prior characterization methods, the direct PnA method does not require estimation of apparent critical parameters of non-identifiable heavy fractions.

1. Introduction

The interaction of fluid flow with phase behavior can be significant in many petroleum reservoir processes, such as hydrocarbon-gas, CO_2, and steam injection. Reliable design of these reservoir processes requires compositional simulation, where the fluid system is characterized using a cubic equation of states (EOS). Widely used EOSs in the petroleum industry include the Peng–Robinson (PR) EOS (Peng and Robinson, 1976, 1978) and the Soave-Redlich-Kwong (SRK) EOS (Soave, 1972). These EOSs along with the van der Waals (vdW) mixing rules, when properly used, give reasonable accuracy and high computational efficiency (Ikeda and Schaefer, 2011).

Reservoir fluids contain a large number of compounds, most of which are non-identifiable. They are reported as single carbon number (SCN) fractions and a lumped fraction (a plus fraction; e.g., the heptane-plus fraction or C_{7+}) in a compositional analysis. The

* Corresponding author at: 3-114 Markin/CNRL Natural Resources Engineering Facility, University of Alberta, Edmonton, AB, Canada T6G 2W2.
Tel.: +1 780 492 6121; fax: +1 780 492 0249.
E-mail address: rokuno@ualberta.ca (R. Okuno).

http://dx.doi.org/10.1016/j.ces.2015.01.032
0009-2509/

uncertainties associated with non-identifiable compounds are more significant for heavier reservoir fluids because their fractions are higher. Even for a well-defined series of *n*-alkanes, for example, critical points are uncertain for carbon numbers (CNs) higher than 36 (Nikitin et al., 1997). Also, different types of hydrocarbons are present within each SCN fraction, such as paraffins (P), napthenes (N) and aromatics (A). Their concentrations and critical properties are unknown.

A conventional procedure for reservoir fluid characterization using an EOS is to adjust various EOS-related parameters to match the experimental data available, such as bubble- and dew-points and densities. The adjustment parameters often used include critical temperature (T_C), critical pressure (P_C), acentric factor (ω), volume-shift parameters, and binary interaction parameters (BIPs). The constant terms for the attraction (a) and covolume (b) parameters, Ω_a and Ω_b, are also sometimes used as adjustment parameters. Since the relationship between these EOS-related parameters and phase behavior predictions is rather implicit and non-linear, matching the experimental data available does not always yields a reliable fluid model that is accurate at thermodynamic conditions away from experimental conditions. This is true especially when many EOS-related parameters are simultaneously regressed to the available experimental data. Thus, the correlative accuracy of a fluid model does not necessarily mean the predictive capability.

How phase behavior predictions can be controlled through a cubic EOS is not fully understood in the literature. Phase behavior predictions using a cubic EOS depend on the attraction (a) and covolume (b) parameters. When BIPs are used for a mixture, they affect the phase behavior predictions through the mixing rules used. It is obvious that phase behavior predictions can be controlled more directly by the attraction and covolume parameters than by T_C, P_C, and ω. Current practice of reservoir fluid characterization mentioned above does not effectively utilize the original simplicity of cubic EOSs.

For single-component fluids, various researchers conducted direct adjustment of the attraction and covolume parameters. Thodos (1955a) estimated the attraction and covolume parameters of the vdW EOS for *n*-alkanes using a group contribution method. The approach was later applied to unsaturated aliphatic, naphthenes, and aromatics (Thodos, 1955b, 1956, 1957). Deriving T_C and P_C from the attraction and covolume parameters is straightforward in this case since the vdW attraction parameter does not depend on temperature. Tsonopoulos and Wilson (1983), Heidman et al. (1985), Enick et al. (1987) and Economou et al. (1997) directly adjusted the attraction and covolume parameters of an EOS to match the vapor pressure and liquid density data for water. They used the Zudkevitch and Joffe (1970) modification of the Redlich–Kwong EOS. Optimization of components' parameters to match vapor pressure and liquid density data has been also performed with other types of EOSs (Voutsas et al., 2006; Aparicio-Martínez and Hall, 2006).

Ahmed and Meehan (2010) developed correlations for the attraction and covolume parameters of the PR EOS for the C_{7+} fraction as a single component. They generated 49 hypothetical plus-fractions based on the correlations of Riazi and Daubert (1986) for molecular weight (MW), boiling point (T_b), and specific gravity (γ). For each fraction, 100 densities were specified in pressure–temperature space. The attraction and covolume parameters adjusted to match the densities were correlated with MW, T_b, and γ. Their correlations were recommended for density prediction of crude oil and gas condensate. Their EOS models exhibited significant improvement in phase behavior predictions for gas condensates and oils without volume shift. They concluded that splitting of a plus fraction was not required. Although saturation pressures were matched by adjusting BIPs, their approach was not tested in term of the predictive capability of compositional phase behavior, such as minimum miscibility pressures, swelling test, and gas solubilities.

Characterization of a plus fraction using multiple pseudo components becomes important when an EOS model is used not only to predict phase densities, but also to simulate vaporization and condensation of intermediate components in various enhanced oil recovery processes. To the best of our knowledge, however, no method has been presented in the literature that directly adjusts the attraction and covolume parameters of a cubic EOS to characterize volumetric and compositional phase behavior of petroleum reservoir fluids.

The attraction and covolume parameters have been indirectly adjusted through T_C, P_C, and ω in prior characterization methods. This is likely because the attraction and covolume parameters are not measurable and EOS-specific. However, this is also true for T_C, P_C, and ω for non-identifiable compounds in fluid characterization using an EOS. Each of SCNs and plus fractions contains a number of different compounds, such as the paraffinic, naphthenic, and aromatic compounds, with unknown concentrations. Furthermore, these fractions are grouped into a few pseudo components so that EOS computations are efficient in reservoir flow simulation. Therefore, apparent properties (e.g., T_C, P_C, and ω) of pseudo components are only estimated, and even extrapolated for high-CN fractions. It is difficult to justify the reliability of the estimated critical properties in the absence of measured values. Also, the parameter values estimated for pseudo components are usually adjusted to correlate experimental data based on the EOS used. Thus, the properties of these components eventually become EOS-specific.

A characterization method was recently presented in our previous publications (Kumar and Okuno, 2013) based on the concept of perturbation from *n*-alkanes (PnA). Instead of attempting to estimate apparent critical properties of pseudo components, the PnA method first assigned the pseudo components the optimized T_C, P_C, and ω values with which the PR EOS gives accurate predictions of vapor pressures and liquid densities for *n*-alkanes. Then, they were perturbed from the *n*-alkane values in well-defined directions until the saturation pressure and liquid density data at the reservoir temperature were matched. The perturbation was conducted in the increasing direction for T_C and P_C, and in the decreasing direction for ω to make the pseudo components gradually more aromatic. The perturbation also controlled the qualitative trend of the ψ parameter ($\psi = a/b^2$) with respect to CN. This ensured that the attraction (a) and covolume (b) parameters for each pseudo component had proper interrelationship depending on the CN range of pseudo components. Extensive testing of the PnA method by use of 77 different reservoir fluids showed that various types of phase behavior were accurately predicted once the saturation pressures and liquid densities were matched.

The PnA method did not require volume shift to match densities for the fluids studied. This is desirable for the following reasons; (i) when used as adjustment parameters, volume shift affects phase behavior predictions at the thermodynamic conditions that the available PVT data do not cover (Kumar and Okuno, 2013, 2014), and (ii) volume shift parameters cannot be canceled out from the fugacity equations, if the effect of capillary pressures is significant on the equations. The second reason is becoming important considering the increasing interests in hydrocarbon recovery from tight/shale reservoirs, where pore geometries affect phase behavior (Schulte, 1980; Whitson and Belery, 1994; Nojabaei et al., 2013).

In this research, the PnA method is simplified by directly perturbing the attraction and covolume parameters, instead of T_C, P_C, and ω, for reservoir fluid characterization by use of the PR EOS. The development of the direct PnA method begins by establishing the attraction and covolume parameters for *n*-alkanes up to $n\text{-}C_{100}$. The effects of aromaticity on the a, b, and ψ parameters are then discussed. A new algorithm developed for reservoir fluid characterization controls phase behavior predictions through direct perturbation of the b and ψ parameters. The algorithm is applied to 84 different reservoir fluids, for which phase behavior data are available

in the literature. Results show the reliability, robustness, and simplicity of the direct PnA method.

2. Attraction and covolume parameters for hydrocarbons

T_C, P_C, and ω for n-alkanes from n-C_7 through n-C_{100} were optimized in terms of liquid densities and vapor pressures by use of the PR EOS (Kumar and Okuno, 2012). As presented in the Supporting information (Part 1), it has been confirmed that the PR attraction and covolume parameters for n-alkanes based on Kumar and Okuno (2012) are suitable for the direct perturbation in this research.

In the previous PnA method (Kumar and Okuno, 2013), the perturbations of T_C, P_C, and m were conducted from the n-alkane values towards a higher level of aromaticity to match the saturation pressure and liquid densities at a given reservoir temperature. This is essentially to perturb the attraction and covolume parameters from n-alkane values in the direction of increasing level of aromaticity, but only indirectly. The effect of aromaticity on the parameters and proper interrelationship between the attraction and covolume parameters (Kumar and Okuno, 2013) are briefly explained in the Supporting information (Part 2). The term "aromaticity" was defined by Yarborough (1979) as the percentage of total carbon atoms in a molecule, which are within the benzene ring. Yarborough (1979) presented trend curves for specific gravity at 288.15 K and 1.01325 bar as a function of CN and aromaticity. In his presentation, CN ranged from 7 to 40, and aromaticity from 0 to 80, as reproduced in the Supporting Information (Part 2, Fig. S12).

In Kumar and Okuno (2013), these trend curves were successfully used to explain how perturbation of critical parameters (equivalently, the attraction and covolume parameters) should be done for the different CNs. Details were presented in Kumar and Okuno (2013) and summarized in the Supporting information (Part 2). In the current paper, the same knowledge is used to guide the direct perturbation of the attraction and covolume parameters.

The attraction parameter increases with CN for a fixed aromaticity level (Fig. S13). The effect of aromaticity on the attraction parameter is not systematic; i.e., the attraction parameter increases with aromaticity for light hydrocarbons, and the trend is the other way around for heavier hydrocarbons. The trend of the covolume parameter is more systematic (Fig. S14). The covolume parameter for n-alkane is higher than that for aromatic hydrocarbons for a given CN. Also, n-alkanes exhibit the largest gradient of the covolume parameter with respect to CN. Note that aromaticity should be interpreted as qualitative deviation from n-alkanes within this research.

One of the most important parameters in the PnA method is $\psi = a/b^2$, or

$$\psi = \frac{\Omega_a}{\Omega_b^2} P_C \left(1 + m\left[1 - \left(\frac{T}{T_C}\right)^{0.5}\right]\right)^2 \tag{1}$$

on the basis of the PR EOS. The ψ parameter is sensitive to the level of aromaticity for light and intermediate hydrocarbons (Fig. S15). The ψ parameter monotonically decreases with CN for high aromaticity levels, but exhibits a maximum for low aromaticity levels, including n-alkanes. The ψ parameter for a fixed CN increases with increasing level of aromaticity, and changes its sensitivity to aromaticity around CN 20. The ψ parameter is useful in controlling variable perturbation at different CNs.

3. Direct perturbation of the attraction and covolume parameters

The development of the direct PnA method was motivated by the question as to how many parameters are required to represent phase behavior of reservoir fluids on the basis of the PR EOS with the vdW mixing rules. A detailed investigation of phase behavior predictions from the PR EOS has indicated that the volumetric and compositional phase behaviors are largely determined by the covolume and ψ parameters, respectively. Also, these parameters for the pseudo components of a given fluid can be controlled systematically by a few adjustment parameters. The objective of this section is to present a fluid-characterization algorithm that reflects our findings regarding systematic control over phase behavior predictions through the PR EOS.

In the subsequent subsections, a new set of equations is first presented for perturbation of the covolume and ψ parameters in MW space. Then, a new algorithm is presented that uses the equations to match experimental data in reservoir fluid characterization.

3.1. Equations for direct perturbation

Fig. S14 in the Supporting information shows the covolume parameters calculated on the basis of Eqs. (S8) and (S9). The covolume values for n-alkanes can be correlated with MW as follows:

$$b = -14.6992113939827 + 1.36977232166027(\mathrm{MW}) - 9.12089276536298 \times 10^{-5}(\mathrm{MW})^2. \tag{2}$$

As shown in Fig. S14, the covolume parameter for a given pseudo component tends to decrease as it becomes more aromatic. Also, the effect of aromaticity on the covolume parameter tends to be more significant for a heavier component. The following equation can accommodate these desired trends with respect to the f_b perturbation parameter:

$$b_i = -14.6992113939827 + 1.36977232166027(\mathrm{MW}_i/m_{bi}) - 9.12089276536298 \times 10^{-5}(\mathrm{MW}_i/m_{bi})^2, \tag{3}$$

where i is the index for pseudo components and $m_{bi} = (\mathrm{MW}_i/86.0)^{f_b}$. The f_b perturbation parameter is zero for n-alkanes, and increases with increasing level of aromaticity in terms of volumetric phase behavior. The m_{bi} parameter increases with MW for a given f_b value. When a pseudo component has a MW of 86.0, which corresponds to the MW of n-hexane, the m_{bi} parameter is unity regardless of the f_b value applied uniformly to all pseudo components within a given fluid.

Fig. S15 shows the qualitative trends of the ψ parameters for two model fluids. The lighter model fluid exhibits an increasing trend, while the heavier model fluid exhibits a decreasing trend with respect to MW. The indirect PnA method of Kumar and Okuno (2013) resulted in non-linear ψ curves with respect to MW. However, an extensive testing of the method has indicated that the ψ parameter can be linear with respect to MW without loss of reliability. Thus,

$$\psi_i = g(\mathrm{MW}_i - \mathrm{MW}_1) + C\psi_{n1}, \tag{4}$$

where MW_1 is the MW of the lightest pseudo component ($i=1$), and g is the gradient of ψ with respect to MW. $C\psi_{n1}$ represents the ψ parameter for the lightest pseudo component as a product of the C multiplier and the ψ parameter for the lightest pseudo component as an n-alkane (ψ_{n1}). The value of ψ_{n1} is calculated by use of Eq. (1) with T_C, P_C, and m from Kumar and Okuno (2012); that is, MW_i and ψ_{n1} are constants for a given fluid once the compositional characterization is conducted. Then, the ψ parameter in MW space can be perturbed through g and C.

Perturbation of the ψ parameters is not as straightforward as that of the covolume parameters through Eq. (3). This is because the ψ trend depends on the CN range of pseudo components, the level of aromaticity, and temperature. Therefore, a perturbation scheme for ψ has been developed on the basis of a set of the f_b, g, and C parameters that were optimized for 74 different reservoir

fluids. Four pseudo components were used for their plus fractions as in Kumar and Okuno (2013). The gradient (i.e., g in Eq. (4)) was represented by the summation of f_b and f_ψ. The C multiplier in Eq. (4) was split into two parts; c that is independent of f_b, and c' that is linear with f_b with zero intercept.

Out of the 74 fluids, 54 fluids were light, where density data were well represented by f_b of zero. Thus, they behave as n-alkanes in terms of volumetric phase behavior. The C parameters optimized for these 54 light fluids correspond to the c part, which is considered to represent the effects of the CN range of pseudo components and temperature on the C multiplier. They were correlated with MW_1 and temperature as follows:

$$c = 0.1088\left[(T_r)^{1.0405} + (M_r)^{1.2656}\right] + 0.5825, \tag{5}$$

where T_r is the reservoir temperature (T_{RES}) in Kelvin divided by 277.0, and M_r is MW_1 divided by the MW of n-heptane (100.2 g/mol). The absolute average deviation (AAD) of Eq. (5) from the c values for the 54 fluids is 4.5%. Eq. (5) does not need to be very accurate since it will be part of the regression algorithm that has a few adjustable parameters to match experimental data. This is also true for the c' part of the C multiplier to be described below.

For the 20 heavier fluids out of the 74 reservoir fluids, f_b was positive, representing the effect of aromaticity on volumetric behavior predictions. To extract the c' part from the C multipliers optimized for these 20 fluids, the c values calculated by use of Eq. (5) were subtracted from the optimized C multipliers. Then, the resulting c' part, which is considered to represent the aromaticity effect on the C multiplier, was correlated as follows:

$$c' = \left[\frac{1.0998(f_b + f_\psi)}{P_r} + 0.1763\right] Z_{SAT} f_b. \tag{6}$$

Z_{SAT} is the liquid compressibility factor calculated at the experimental saturation pressure (P_{SAT}) at T_{RES}. P_r is the saturation pressure at T_{RES} under the assumption that the pseudo components are n-alkanes, divided by P_{SAT}. The calculation of P_r requires the PR EOS with T_C, P_C, and m from Kumar and Okuno (2012) and P_{SAT}. Fig. 1 shows the quality of Eq. (6) in correlating $c'/Z_{SAT}f_b$ with $(f_b+f_\psi)/P_r$. Although the AAD of Eq. (6) for the 20 fluids is 35%, it is successfully used in the regression processes with f_b and f_ψ as will be shown later.

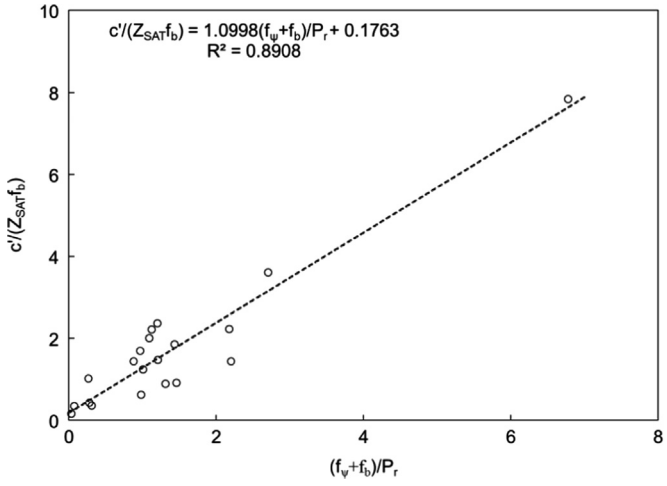

Fig. 1. Correlation of $c'/Z_{SAT}f_b$ with $(f_b+f_\psi)/P_r$ using a linear function. For each of the 20 data points, c' is obtained by subtracting the c value calculated from Eq. (5) from the optimized C multiplier. The 20 fluids considered are not light, and their f_b values are positive.

Eq. (4) is then rewritten as

$$\psi_i = g(MW_i - MW_1) + C\psi_{n1} = (f_b + f_\psi)(MW_i - MW_1) + (c + c')\psi_{n1} \tag{7}$$

in this research. Obviously, this is only one of many possible ways to use the linear form of the ψ parameter in MW space. Eqs. (3) and (7) are simple, but flexible enough for perturbation of the f_b, g, and C parameters in reservoir fluid characterization as presented in the next subsection.

A single value is assigned to each of the perturbation parameters f_b, g, and C for a given fluid. However, the different levels of aromaticity for different components within a fluid have been considered in the development of Eq. (3) for covolume by using m_{bi}. As shown in the Supporting information (Part 2), the aromaticity effect on the attraction parameter through ψ is not as systematic as that on covolume. As will be also shown in Section 4, this is likely because the trend of pseudo components' attraction parameters depends not only on aromaticity, but also on temperature and CNs.

3.2. Algorithm

The algorithm presented in this research is kept as simple as possible. The covolume parameters are perturbed by use of Eq. (3) through f_b. The ψ parameters are perturbed by use of Eq. (7) through g and C, or through f_b, f_ψ, and c. Note that c is adjustable to some extent because it is not exact as the C multiplier when f_b is zero, as mentioned previously. The data to be matched are the P_{SAT} at T_{RES} and liquid density data at T_{RES} at different pressures. Other available data are saved for testing the predictive capability of the resulting fluid models, such as minimum miscibility pressures (MMPs), and liquid saturation curves from constant volume depletion (CVD) and constant composition expansion (CCE).

The algorithm consists of two nested loops as shown in the flow chart, Fig. A 1, in Appendix A. The inner loop is to match the P_{SAT} by adjusting f_ψ in Eq. (7) for a set of f_b and c given by the outer loop. The initial value for f_ψ is zero, and f_ψ is adjusted by Δf_ψ per iteration (e.g., $\Delta f_\psi = 0.0001$). The sign for Δf_ψ (i.e., $+\Delta f_\psi$ or $-\Delta f_\psi$) is negative if the saturation pressure is calculated to be higher than the experimental value. Otherwise, it is positive.

The outer loop is to match density data by adjusting either c in Eq. (7) or f_b in Eqs. (3) and (7). Adjustment of c is first attempted to see if the deviation of density predictions is entirely attributed to the c correlation (Eq. (5)); that is, f_b is always zero when c is adjusted. Adjustment of c is made by Δc (e.g., $\Delta c = 0.001$) in each iteration. The sign for Δc (i.e., $+\Delta c$ or $-\Delta c$) is determined to make the average deviation (AD) of density predictions smaller. Once the sign is determined in the first iteration step, it can be kept for the subsequent iteration steps until the AD changes its sign because the relationship between the density AD and c is monotonic within the range of investigation in this research. Fig. 2 shows the monotonic change of the density AD with respect to c for two example cases. The zero deviation can be obtained by either $+\Delta c$ or $-\Delta c$.

It is not always possible to achieve zero density AD by adjusting c with zero f_b. This is because the covolume parameters should be adjusted for heavy hydrocarbon mixtures, for which the PR EOS tends to underpredict liquid densities (Søreide, 1989; Kumar and Okuno, 2014). It has been observed that, with the fluids examined, c is between 0.75 and 1.20 when the correction of c with zero f_b can achieve zero density AD. If this does not occur, c is overwritten by the original value based on Eq. (5), and adjustment of f_b is initiated. The initial value for f_b is zero, and f_b is increased by Δf_b per iteration (e.g., $\Delta f_b = 0.0001$).

The example values given for Δf_b, Δc, and Δf_ψ in previous paragraphs are sufficient to match the P_{SAT} and densities. To

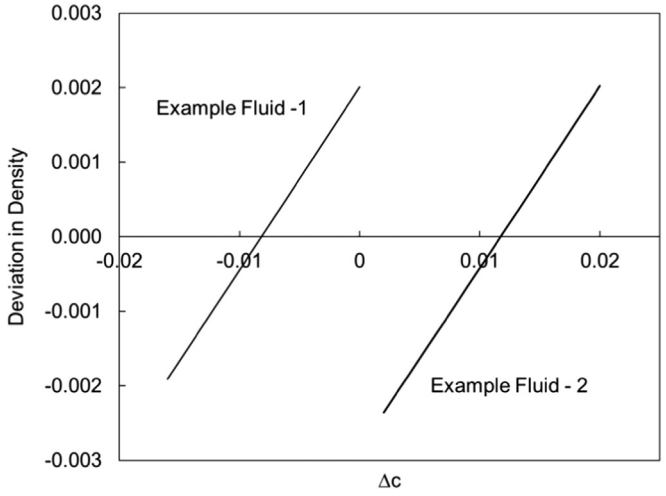

Fig. 2. Average deviations of density predictions from experimental data during the regressions for two different fluids. Density matching is achieved by adjustment of the c parameter for light fluids. For example fluid 1, the c parameter is decreased from the value calculated using Eq. (5). For example fluid 2, it is increased from the value calculated using Eq. (5), in order to obtain the density match.

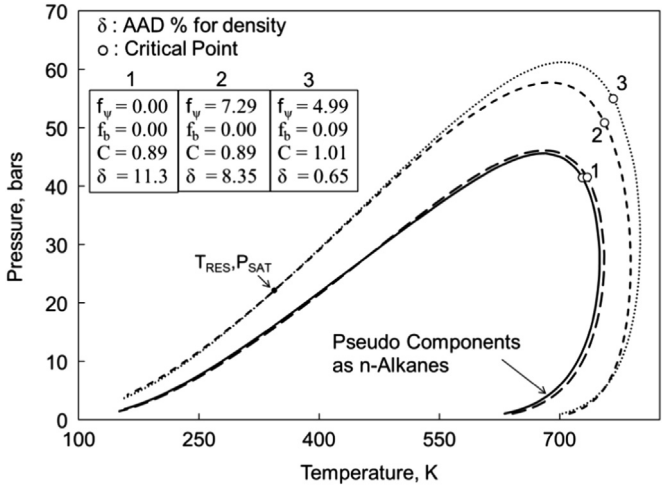

Fig. 3. Variation of the phase envelope in P–T space during the PnA regression for a fluid of 42°API. Curve 1 represents the phase envelope at the initialization of the algorithm, where f_ψ and f_b are zero. Curve 2 is the phase envelope when P_{SAT} is matched by adjusting f_ψ (i.e., densities have not been matched yet). Curve 3 shows the final phase envelope when P_{SAT} and densities are matched, as indicated by the value of δ. Curves 1, 2, and 3 are also compared with the solid curve that represents the phase envelope when the pseudo components are assumed to be n-alkanes with T_C, P_C, and ω from Kumar and Okuno (2012). As the regression proceeds, the critical point becomes higher, and the phase envelope accordingly becomes greater in P–T space.

reduce the number of iterations, however, these values can be made proportional to the AD during regression.

A step-wise description of the algorithm is as follows:

Step 1. Composition characterization
On the basis of the compositional data available, the plus fraction is split into n pseudo components using the chi-squared distribution function. Details can be found in Quiñones-Cisneros et al. (2004). The i subscript is the index for pseudo components; $i=1, 2,\ldots,n$.
Step 2. Calculation of c, P_r, Z_{SAT}, and ψ_{n1}
Eqs. (5)–(7) require c, P_r, Z_{SAT}, and ψ_{n1} to be calculated. The definitions of these variables were given in Section 3.1.
Step 3. Adjustment of the covolume and ψ parameters for the pseudo components

The iteration index is j for f_ψ and k for f_b. $j=k=1$.

(1) $f_b=f_\psi=0.0$
(2) Calculate the covolume parameters ($b_{i,k}$) by use of Eq. (3).
(3) Calculate the ψ parameters ($\psi_{i,j,k}$) by use of Eqs. (6) and (7).
(4) Calculate the attraction parameters ($a_{i,j,k}$) as $a_{i,j,k}=\psi_{i,j,k}\times(b_{i,k})^2$.
(5) Calculate the saturation pressure (P_{SATCAL}) at T_{RES}. Calculate $\varepsilon=|P_{SATCAL}-P_{SAT}|/P_{SAT}$. If $\varepsilon<\varepsilon_{TOL}$, go to Step 3(6) with $j=1$. Otherwise, f_ψ is adjusted. $f_\psi=f_\psi+\Delta f_\psi$ if $P_{SATCAL}-P_{SAT}<0$. Otherwise, $f_\psi=f_\psi-\Delta f_\psi$. $j=j+1$ and go to Step 3(3). ε_{TOL} is 0.0001 in this research.
(6) Calculate densities at T_{RES} and the experimental pressures. Calculate the AAD (δ) of the densities calculated. If $\delta<\delta_{TOL}$, stop. Otherwise, adjust either c or f_b as described earlier in this subsection; go to Step 3(1) with $c=c\pm\Delta c$, or Step 3(2) with $f_b=f_b+\Delta f_b$, $f_\psi=0$, and $k=k+1$. δ_{TOL} is 0.1% in this research.

The algorithm does not require T_C, P_C, and ω for the pseudo components in the fluid model of interest, in contrast to the indirect PnA algorithm (Kumar and Okuno, 2013). The new algorithm took approximately 3 seconds to conduct characterization of a fluid, while the previous algorithm for the indirect PnA method took a few minutes. Both algorithms were written in FORTRAN and based on exhaustive search methods, instead of gradient-based methods. The computations were performed on the Intel Core i7-960 processor at 3.20 GHz and 8.0 GB RAM.

Appendix B describes the approach to derive T_C, P_C, and ω from the attraction and covolume parameters for pseudo components. This is useful when one uses commercial software that requires these parameters as input information.

3.3. Variation of phase behavior during regression

The direct PnA algorithm systematically controls the attraction and covolume parameters for the pseudo components through f_ψ and f_b, or f_ψ and c. This subsection shows how two-phase behavior in P–T space for a given fluid varies with the adjustment parameters during the regression process. Fig. 3 shows an example for a fluid of 42°API. Curve 1 represents the phase envelope at the initialization of the algorithm, where f_ψ and f_b are zero. Curve 2 is the phase envelope when P_{SAT} is matched by adjusting f_ψ (i.e., densities have not been matched yet). Curve 3 shows the final phase envelope when P_{SAT} and densities are matched, as indicated by the value of δ. Curves 1, 2, and 3 are also compared with the solid curve that represents the phase envelope when the pseudo components are assumed to be n-alkanes with T_C, P_C, and ω from Kumar and Okuno (2012). As the regression proceeds, the critical point becomes higher, and the phase envelope accordingly becomes greater in P–T space.

Fig. 4 shows a similar example for a light fluid, where densities are matched by adjusting c with $f_b=0.0$. Unlike in the previous example, the variation of the critical point is irregular as the regression proceeds from curve 1 to 3. This may be because this particular fluid behaves as an n-alkane mixture in terms of volumetric phase behavior, and the effect of aromaticity on two-phase behavior is not as obvious as the previous example fluid. Nevertheless, curve 3 entirely contains the n-alkane envelope, as in the previous example. This is the common observation made in all fluids examined so far.

4. Case studies

In this section, the direct PnA method is applied to 84 different reservoir fluids, for which experimental data are available in the

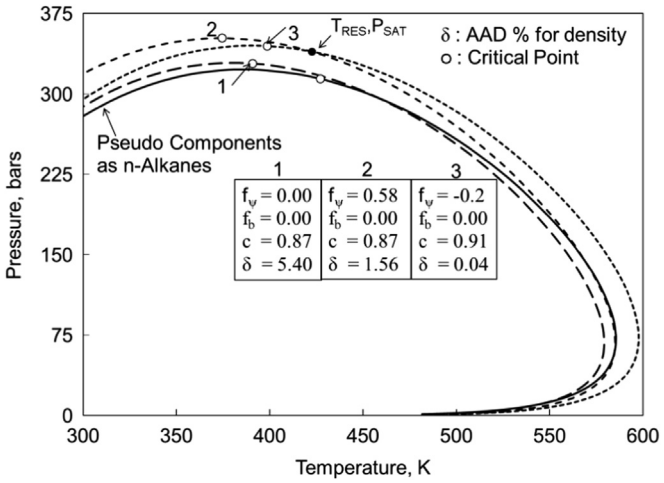

Fig. 4. Variation of the phase envelope in P–T space during the PnA regression for a light fluid, where densities are matched by adjusting c with f_b=0.0. Curve 1 represents the phase envelope at the initialization of the algorithm, where f_ψ is zero. Curve 2 is the phase envelope when P_{SAT} is matched by adjusting f_ψ (i.e., densities have not been matched yet). Curve 3 shows the final phase envelope when P_{SAT} and densities are matched, as indicated by the value of δ. Curves 1, 2, and 3 are also compared with the solid curve that represents the phase envelope when the pseudo components are assumed to be n-alkanes with T_C, P_C, and ω from Kumar and Okuno (2012). Curve 3 entirely contains the n-alkane envelope, as in the previous example given in Fig. 3.

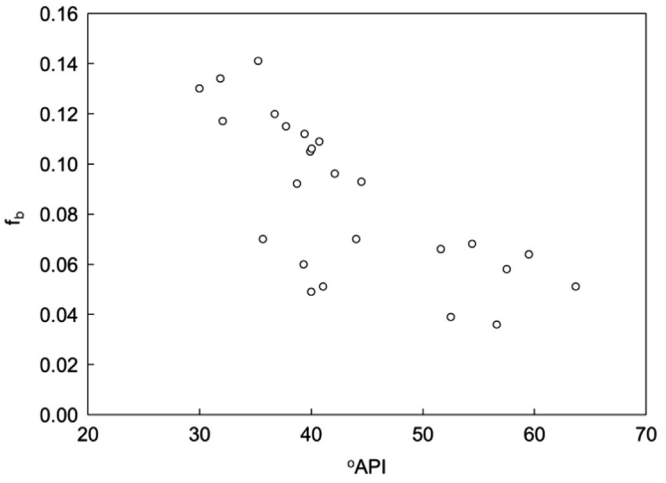

Fig. 5. The converged f_b value tends to increase with increasing specific gravity of the fluid characterized. f_b is representative of the aromaticity level; it is zero for n-alkanes and increases with increasing aromaticity level.

literature. They are 47 gas condensates, 33 conventional oils, and 4 heavy oils. As mentioned previously, the direct PnA algorithm is to match the P_{SAT} at T_{RES} and liquid densities at T_{RES} and different pressures using f_ψ and f_b, or f_ψ and c. Matching of densities tends to be conducted by c for light fluids, and by f_b for heavier fluids. f_ψ mainly controls compositional phase behavior, which consequently affects volumetric phase behavior. Available data other than those used in the regression process are used to test the predictive capability of the resulting fluid models. For example, CVD liquid saturation data are available for 34 gas condensates and 7 conventional oils. The other 18 conventional oils have MMP data, one of which is a corrosive volatile oil containing 19% CO_2. For the heavy oils used, swelling test and phase envelope data are available.

For characterization of light fluids with f_ψ and c, density data for the liquid phase that is equilibrium with the gaseous phase have been found to be more important than single-phase density data. This is plausible because the equilibrium liquid phase is richer in heavy components and more aromatic than the equilibrium gaseous phase and liquid phases in a single-phase region. Capturing the deviation from n-alkanes in the PnA method is more effective with density data of the denser phase. Therefore, simulated liquid density data have been created in two-phase regions for the gas condensates and a few volatile oils on the basis of the fluid models with optimized g and C (see Section 3.1). These optimized models accurately reproduce measured single-phase density data with an AAD of less than 1%; that is, the consistency has been retained between the measured and simulated density data for each of these light fluids.

The number of components is 12 throughout this research, four of which are pseudo components for C_{7+}. The others are N_2, CO_2, C_1, C_2, C_3, C_4, C_5, and C_6, where grouping of n- and i-alkanes is based on the conventional mass-based mixing rule (Pedersen and Christensen, 2007). Unless otherwise stated, the BIPs are kept constant as described in Kumar and Okuno (2014); 0.0 for N_2-CO_2, 0.1 for N_2-C_i, where $1 \le i \le 6$, 0.13 for N_2-pseudo-components, 0.1 for CO_2-hydrocarbons, and 0.0 for all hydrocarbon-hydrocarbon pairs.

The converged values for f_ψ and f_b are listed for all tested fluids in separate tables as will be discussed later. f_b is representative of the aromaticity level; it is zero for n-alkanes and increases with increasing aromaticity level. Fig. 5 presents the overall trend that the converged f_b tends to increase with increasing specific gravity of the fluid characterized. However, such a clear trend is not observed for f_ψ. This is because it controls g and C through Eqs. (6) and (7), which are dependent on temperature, aromaticity, and the MW range.

4.1. MMP calculation

The direct PnA method has been applied to characterize the 18 oils given in Table 1. MMP data are available for these oils in the literature. For fluids 14, 16, and 17 in Table 1, MMPs with multiple injection gases were measured. This subsection compares MMPs calculated by the fluid models from the direct PnA method with the corresponding MMP data. This serves as a severe test of the predictive capability of the direct PnA method since an MMP is affected by phase behavior in a wide region of composition space between the oil and injection gas compositions (Egwuenu et al., 2008). The PnA method uses the P_{SAT} and liquid densities at T_{RES} only at the composition of the fluid characterized. Thus, MMPs calculated in this subsection are predictions from the fluid models developed based on the limited data at a point in composition space.

The gravities of the 18 oils range from 31°API to 61°API. Table 1 shows the converged values for f_ψ and f_b. The slope of the ψ parameters with respect to MW is g=f_ψ+f_b as given in Eq. (7). Table 1 presents positive slopes except for Fluid 9. The negative slope of Fluid 9 is expected since only one of the pseudo components is in the CN range less than 20 (see Fig. S15 and Kumar and Okuno, 2013).

MMP calculations were performed by use of the PVTsim version 19.2 (PVTsim, 2010) and PennPVT (Ahmadi and Johns, 2011) software. The calculations with PVTsim based on the method of characteristics were unsuccessful for Fluids 10, 11, 16, and 18. The mixing-cell method within PennPVT was used for these fluids and Fluid 17. AADs of the calculated MMPs are listed in Table 1. Table 2 presents ADs for all injection gases for Fluid 17. For the cases given in Tables 1 and 2, the calculations resulted in an overall AAD of 6.4%, which is reasonable considering uncertainties such as the effect of dispersion on the experimentally determined MMPs. Adjustment of BIPs can improve the calculated MMPs especially when non-hydrocarbon components are present at high concentrations. This will be discussed in Section 5.

Table 1
Converged f_ψ, f_b, and p values for reservoir oils characterized using the direct PnA method. Slim-tube MMPs are reported for these oils in the literature.

Oil nos.	References	MW (g/mol)	°API	Res. temp. (K)	No. of density data	f_ψ	f_b	p	% AD MMP prediction
1	Jaubert et al. (2002), F1	135.24	35.22[‡]	374.85	5	0.4223	0.1411	4.5	5.60
2	Jaubert et al. (2002), F2	136.25	39.89	372.05	6	1.0947	0.1051	4.7	14.28
3	Jaubert et al. (2002), F3	82.41	39.31[‡]	387.35	11	0.8280	0.0690	6.3	1.27
4	Jaubert et al. (2002), F4	63.17	40.34[‡]	388.20	7	0.1683	0.074[x]	3.0	0.09
5	Jaubert et al. (2002), F5	125.82	32.04[‡]	394.25	12	0.8105	0.1171	4.5	0.55
6	Jaubert et al. (2002), F6	96.25	37.73[‡]	383.15	5	0.6294	0.1151	4.2	5.76
7	Jaubert et al. (2002), F7	96.19	41.06[‡]	393.15	12	1.6151	0.0520	4.9	1.29
8	Jaubert et al. (2002), F11	82.55	38.71[‡]	373.75	11	0.6737	0.0921	3.8	8.96
9	Jaubert et al. (2002), F13	150.2	35.64[‡]	377.55	8	−0.2542	0.0701	4.4	2.65
10	Al-Ajmi et al. (2011), F1	161.42	31.85	350.40	16	0.6427	0.1341	4.6	12.45
11	Al-Ajmi et al. (2011), F2	109.37	40.03	353.70	17	0.7924	0.1061	3.9	14.56
12	Ekundayo (2012)	86.57	51.60	402.59	7	1.1011	0.0671	4.6	3.03
13	Wijaya (2006)	113.90	44.00	302.59	17	1.3260	0.0701	4.5	9.94
14	Høier (1997), System 1[¥]	97.0	39.40	368.15	6	0.6933	0.1121	4.4	8.01
	Høier (1997), System 2[¥]	97.0	39.40	368.15	6			4.4	4.54
	Høier (1997), System 3[¥]	97.0	39.40	368.15	6			4.4	4.81
	Høier (1997), System 4[¥]	97.0	39.40	368.15	6			4.4	5.37
15	Lindeloff et al. (2013), Oil A	148.24	30.00[‡]	329.26	10	1.0253	0.1301	4.6	12.25
16	Graue and Zana (1981)[#]	177.0	42.10	344.26	1	4.8227	0.0971	7.7	5.15
	Graue and Zana (1981)[#]	177.0	42.10	344.26	1			7.7	9.16
17	Clark et al. (2008)	53.87	47.00	413.70	12	0.7289	0.1591	3.0	6. 80[*]
18	Negahban et al. (2010)	101.90	40.00	394.00	16	1.1901	0.0491	4.8	5.62

[x] Δc value (f_b is zero).
[‡] As reported. All other API gravities are calculated from the density at 288.15 K and 1.01325 bar.
[¥] Oil composition and saturation data used were taken from Whitson and Belery (1994). Systems 1–4 indicate four different injection gases.
[#] %ADs of 5.15 and 9.16 are for injection gases 1 and 2, respectively.
[*] AAD for 26 different injection gases is 6.8%. Deviations for these injection gases are shown in Table 2.

Table 2
Deviations for MMP predictions for volatile oil 17 (Clark et al., 2008) based on the direct PnA method of volatile oil.

Injection gas (mol%)[a]	Dev. %	Injection gas (mol%)[a]	Dev. %	Injection gas (mol%)[a]	Dev. %	Injection gas (mol%)[a]	Dev. %
CO_2 (100)	5.26	CO_2 (95)+C_2 (5)	4.85	CO_2 (95)+C_5 (5)	−7.83	CO_2 (95)+N_2 (5)	0.18
CO_2 (95)+C_1 (5)	6.47	CO_2 (90)+C_2 (10)	4.53	CO_2 (90)+C_5 (10)	−17.34	CO_2 (90)+N_2 (10)	−3.44
CO_2 (90)+C_1 (10)	6.47	CO_2 (85)+C_2 (15)	5.35	CO_2 (85)+C_5 (15)	−20.67	CO_2 (85)+N_2 (15)	0.48
CO_2 (85)+C_1 (15)	6.94	CO_2 (80)+C_2 (20)	5.70	CO_2 (80)+C_5 (20)	−1.56	CO_2 (80)+N_2 (20)	3.57
CO_2 (80)+C_1 (20)	6.87	CO_2 (75)+C_2 (25)	7.62	CO_2 (75)+C_5 (25)	5.67	CO_2 (75)+N_2 (25)	7.59
CO_2 (75)+C_1 (25)	6.86	CO_2 (70)+C_2 (30)	9.55	CO_2 (70)+C_5 (30)	6.30	CO_2 (70)+N_2 (30)	10.78
CO_2 (70)+C_1 (30)	5.00					N_2 (100)	13.75

[a] Numbers inside bracket shows mol% of the component in injection gas.

4.2. Gas condensates

Table 3 presents the 47 gas condensates tested, for which MWs range from 19.75 g/mol to 54.92 g/mol. Gas condensates 6, 7, 8, 11, 12, 36, and 38 are near critical at their reservoir conditions. The regression was conducted by f_ψ and c with zero f_b for all the gas condensates. The values listed as Δc are the adjustments in c required to match density data. The pseudo components of these gas condensates are in a relatively low CN range between 7 and 30. Therefore, positive slopes of ψ with respect to MW are observed for 42 gas condensates in Table 3. Note that $g=f_\psi+f_b=f_\psi$ since f_b is zero for these fluids.

Data types available for the gas condensates are indicated as 1 for CVD liquid saturations, 2 for CCE liquid saturations, and 3 for CCE relative volumes. The maximum value in these experimental data is listed for each of the gas condensates. For example, Fig. 6 shows CVD liquid saturations measured for gas condensate 12 at 387.59 K. It is zero at the dew point of 333.0 bar. The maximum value, 40.90, at 283.7 bar is the value listed for this gas condensate in the second right-most column of Table 3. The equation that defines the deviation is shown below Table 3. Note that the numerator of the equation is given in % with data types 1, 2, and 3. Fig. 6 shows that the predictions from the resulting fluid model are in good agreement with the data. The AAD is calculated to be 0.94% for this case, which is listed in the right-most column of Table 3. Fig. 6 also presents the CVD liquid volume predictions with the conventional characterization method based on Pedersen and Christensen (2007), in which volume shift is used to correct density predictions. This conventional method with volume shifting is referred to as CM_wV, which was described in detail in Kumar and Okuno (2014). The AAD for CM_wV with 12 components is 1.9% for Fig. 6.

Fig. 7 depicts the CCE liquid saturations measured for gas condensate 3 at 382.59 K. The data indicate that the CCE liquid volume first increases gradually, and then decreases with decreasing pressure. The predictions from the EOS fluid model are reasonably accurate, although the deviation at 289.57 bar is relatively large. The AAD is 1.71% with the direct PnA method and 3.7% with CM_wV.

Accurate predictions of volume ratios in CVD and CCE require accurate predictions of both compositional and volumetric phase behavior. The AADs summarized in Table 3 indicate that the fluid models developed by the direct PnA method are reasonable in predicting gas condensates.

4.3. Volatile oils

The direct PnA method has been used to characterize the 15 volatile oils given in Table 4. Oils 10, 12, and 14 are near critical at their reservoir conditions. As mentioned previously in this section, simulated density data for the equilibrium liquid phase were used in the regression for oils 1, 5, 10, 11, 13, 14, and 15. The regression

Table 3
Converged f_ψ, Δc, and p values for gas condensates characterized using the direct PnA method. CVD or CCE data are available for these oils. f_b is zero for these gas condensates.

Fluid nos.	References	MW (g/mol)	°API	Res. temp. (K)	f_ψ	Δc	p	Maximum data value (type[#])	Dev.[¥]
1	Al-Meshari (2004), Fluid-3	31.53	58.3	424.82	0.9774	+0.012	2.0	11.70 (1)	1.42
2	Al-Meshari (2004), Fluid-4	31.44	59.9	403.15	1.4443	−0.016	2.0	13.00 (1)	1.17
3	Al-Meshari (2004), Fluid-5	32.41	60.4	382.59	0.7700	+0.065	2.1	23.36 (2)	1.71
4	Al-Meshari (2004), Fluid-7	36.62	59.6	397.59	2.9688	−0.009	2.6	25.00 (1)	1.51
5	Al-Meshari (2004), Fluid-8	40.77	62.9	424.82	−0.0099	+0.043	2.2	30.40 (1)	0.95
6[ǂ]	Al-Meshari (2004), Fluid-10	39.23	64.7	422.59	−0.2355	+0.043	3.3	33.60 (1)	0.42
7[ǂ]	Al-Meshari (2004), Fluid-11	41.71	62.3	424.82	0.6702	+0.018	3.0	32.20 (1)	1.47
8[ǂ]	Coats and Smart (1986), Gas-5	30.29	61.8	403.70	1.4817	−0.005	2.0	10.40 (2)	0.12
9	Guo and Du (1989), Sample-7	25.53	71.2	406.45	2.1065	−0.033	2.0	5.82 (1)	0.09
10	Imo-Jack (2010)	25.76	54.0	382.59	−4.8869	+0.265	2.2	9.25 (1)	0.85
11[ǂ]	Coats (1985), Recombined	44.40	66.4	435.93	2.0540	+0.020	4.0	32.00 (2)	2.78
12[ǂ]	McVay (1994), Gas B	40.58	58.5	387.59	0.4190	+0.002	2.0	40.90 (1)	0.94
13	Danesh (1998)	27.29	55.3	394.00	1.4306	+0.037	2.0	11.32 (1)	0.27
14	Pedersen and Christensen (2007)	29.14	58.5	428.15	0.0168	+0.120	2.0	11.89 (2)	2.46
15	Hosein et al. (2013), PL-1	23.64	58.9	358.78	2.2649	−0.013	2.0	8.15 (1)	0.48
16	Hosein et al. (2013), PL-2	22.10	52.8	378.15	5.3774	−0.012	2.0	5.08 (1)	0.48
17	Hosein et al. (2013), PL-3	21.55	64.9	357.59	3.6390	−0.097	2.0	4.00 (1)	0.18
18	Hosein et al. (2013), PL-4	20.62	57.3	364.22	4.4763	−0.006	2.0	3.73 (1)	0.32
19	Hosein et al. (2013), PL-5	20.30	64.3	355.37	2.7869	−0.014	2.0	3.79 (1)	0.14
20	Hosein et al. (2013), PL-6	19.75	55.1	367.59	7.9725	−0.016	2.0	1.89 (1)	0.15
21	Moore (1989), CS-1	32.61	71.1	366.48	2.2538	−0.030	2.5	19.90 (1)	0.37
22	Moore (1989), CS-2	35.04	59.7	410.93	1.0086	−0.032	2.0	21.60 (1)	0.35
23	Moore (1989), CS-3	24.45	61.4	365.37	7.2733	−0.015	2.0	2.17 (1)	0.25
24	Whitson and Torp (1983), NS-1	35.04	44.0[ǂ]	410.43	0.9200	−0.023	2.0	21.60 (1)	0.48
25	Whitson and Brulè (2000), GOCW-7	33.62	60.5	358.70	4.8755	−0.008	2.5	23.90 (1)	1.96
26	Drohm et al. (1988), Example-1	54.92	57.1	410.90	1.8164	−0.050	2.9	69.81 (1)	11.34
27	Drohm et al. (1988), Example-2	32.65	59.5	436.70	0.9472	−0.000	2.0	15.63 (1)	0.95
28	Drohm et al. (1988), Example-3	26.26	58.4	393.20	5.1549	−0.022	2.0	4.75 (1)	0.50
29	Drohm et al. (1988), Example-4	28.34	59.0	377.60	3.1677	+0.018	2.1	11.84 (1)	0.49
30	Drohm et al. (1988), Example-5	21.27	56.4	377.60	−0.0195	+0.284	2.0	1.69 (1)	0.09
31	JAPEX	29.81	58.9	402.59	0.9672	+0.000	2.0	6.67 (3)	0.05
32	Pedersen et al. (1988)	26.98	61.82	392.10	4.8159	+0.020	2.1	5.72 (1)	0.62
33	Vogel and Yarborough (1980), Gas-1	36.03	49.6	381.00	0.3244	−0.003	2.2	25.85 (2)	1.49
34	Vogel and Yarborough (1980), Gas-2	30.75	64.6	381.00	1.9861	−0.068	2.1	9.79 (2)	0.69
35	Vogel and Yarborough (1980), Gas-3	23.73	63.2	333.00	−4.0671	+0.280	2.1	3.40 (2)	0.41
36[ǂ]	Whitaker and Kim (1993)	39.34	59.7	366.48	0.2427	+0.061	2.2	47.40 (2)	3.07
37	Kilgren (1966)	36.52	59.5	399.82	0.1825	−0.019	2.1	39.99 (2)	3.83
38[ǂ]	Subero (2009)	40.03	50.5	377.04	1.3835	−0.024	2.1	38.90 (1)	1.03
39	Fawumi (1999)	34.04	57.9	422.59	0.0383	+0.026	2.1	17.16 (1)	1.23
40	Al-Subai (2001), Well-A	32.64	57.4	420.93	0.5792	−0.007	2.6	14.34 (1)	1.60
41	Al-Subai (2001), Well-B	42.44	54.2	424.82	0.2787	−0.012	2.6	32.02 (1)	1.30
42	Al-Subai (2001), Well-D	34.50	63.6	424.82	0.0016	+0.025	2.1	17.17 (1)	1.53
43	Al-Subai (2001), Well-E	23.03	61.4	412.59	5.1525	+0.008	2.1	2.18 (1)	0.35
44	Jacoby et al. (1959)	32.76	63.7	404.82	0.8206	−0.015	2.1	16.10 (2)	1.62
45	Renner et al. (1989)	35.69	63.6	374.82	0.9377	+0.001	2.1	25.02 (2)	1.20
46[ǂ]	Coats (1985), Bottom hole	44.40	67.9	435.93	0.5331	+0.032	4.0	33.49 (2)	1.72
47	Spivak (1971)	27.13	65.6	352.59	0.9568	+0.045	2.1	12.68 (1)	0.98

ǂ As reported. All other API gravities are calculated from the density at 288.15 K and 1.01325 bar.
ǂ Near critical gas condensates.
[#] (1) is CVD liquid saturations (%), (2) is CCE liquid saturations (%), and (3) is CCE relative volumes.
[¥] Deviation is the summation of |experimental value − predicted value| divided by the number of data points.

resulted in positive slopes of ψ with respect to MW for all cases except for oil 12 as indicated in Table 4.

Three types of data available for these oils are given in the second right-most column as 1 for CVD liquid saturations, 2 for CCE liquid saturation, and 3 for CCE relative volumes. This column also shows the measured value at the lowest measured pressure for each fluid. The fluid models developed based on the direct PnA method are able to accurately predict the measured phase behavior. The right-most column of Table 4 indicates the AAD for each fluid. The predicted CCE relative volumes are nearly perfect. The AADs for CVD liquid saturations are relatively large. However, their overall AD is only 1.4%. As a sample result, Fig. 8 gives the comparison between the measured and predicted CVD liquid saturations for near-critical volatile oil 14 at 424.25 K. The value, 42.20, at the lowest measured pressure is listed in the second right-most column for this oil in Table 4. The critical point was measured at 426 K and 388 bar, but it is calculated to be 433.00 K and 389.95 bar by the fluid model based on the PnA method. Although the calculated T_C is 7 K higher than the measured T_C, the CVD liquid saturations are accurately predicted. Fig. 8 also shows the predictions from CM_wV. The critical point calculated with CM_wV is 437.43 K and 393.18 bar. The two methods are reasonably accurate for this case.

4.4. Heavy oils

Four different heavy oils have been characterized by use of the direct PnA method. As shown in Table 5, their API gravities are 19°, 28°, 11°, and 11° for heavy oils 1 to 4, respectively. Heavy oil 2 was classified as a heavy oil on the basis of the definition of Pedersen and Christensen (2007). The heaviest oil considered in this paper is heavy oil 4 with a MW of 482, and the p value in Eq. (S11) is as high as 9.0 for this oil. Table 5 shows that the slope of ψ with respect to MW is negative for this heavy oil.

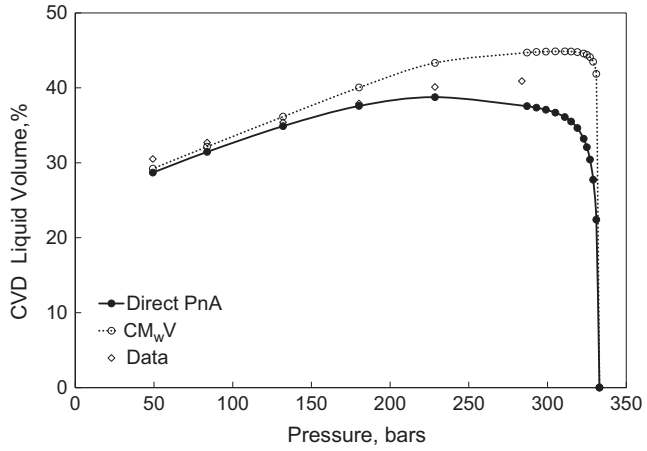

Fig. 6. CVD liquid saturations measured for gas condensate 12 given in Table 3 (McVay, 1994) at 387.59 K. The gas condensate has 11.72 mol% C_{7+}. The MW of the C_{7+} fraction is 169 g/mol, and the overall MW is 40.58 g/mol.

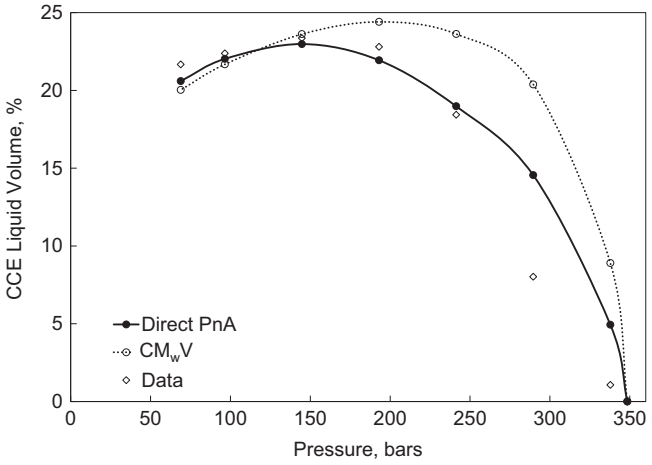

Fig. 7. CCE liquid saturations measured for gas condensate 3 given in Table 3 (Al-Meshari, 2004) at 382.59 K. The gas condensate has 1.81 mol% C_{7+}. The Soave-Redlich-Kwong (SRK) EOS (Soave, 1972) of the C_{7+} fraction is 152.80 g/mol, and the overall MW is 32.41 g/mol.

For heavy oil 1, swelling test data are available for two mixtures at 299.81 K; 60% CO_2 and 40% oil, and 80% CO_2 and 20% oil. Fig. 9 presents predictions of the oleic phase saturation in comparison with the corresponding data for the latter mixture. The AAD for this mixture is 5.2% with the direct PnA method and 6.15% with CM_wV. For pressures higher than 100 bar, the AAD is 2.71% with the direct PnA method and 6.71% with CM_wV. For the former mixture, the AAD with the direct PnA method is 2.2%. CM_wV erroneously predicts a single liquid phase at the highest and second highest pressures. For the lower pressures, the AAD with CM_wV is 5.89%.

For heavy oil 2, saturation pressures measured in swelling tests with CO_2 and a light gas mixture are considered. Fig. 10 compares the predictions with the data presented in Krejbjerg and Pedersen (2006). The AAD is 3.9% for the CO_2 case and 2.8% for the gas mixture case with the direct PnA method. With CM_wV, it is 5.7% for the two injection gases. For heavy oil 3, gas–oil-ratio (GOR) data are available at the reservoir temperature 305.45 K. Fig. 11 shows that the fluid model based on the direct PnA method can accurately predict the GOR for this case. The deviation is relatively high only near the saturation pressure. The AAD is calculated to be 2.9%. The predictions with CM_wV are close to those from the direct PnA method in this case.

For heavy oil 4, the regression in the direct PnA method used the P_{SAT} of 56.64 bar at 347.67 K for the live oil reported (Feed #5 in Li et al., 2013a). Density data for this live oil were unavailable, and, therefore, generated on the basis of the EOS model given by Li et al. (2013a). Fig. 12 presents saturation pressures measured at different temperatures for two mixtures (Feeds #4 and #5 in Li et al., 2013a). Feed #4 is 38.6% CO_2, 36.2% C_3, and 25.2% heavy oil 4 on the molar basis. Feed #5 is 31.7% CO_2, 34.3% n-C_4, and 34.0% heavy oil 4. The fluid model developed by the direct PnA method is reasonably accurate in predicting the saturation pressures in spite of the uncertainties due to the simulated density data that were not validated against any data. The AAD of the saturation pressure predictions is 13.7% for Feed #4 and 6.0% for Feed #5. If the BIPs for CO_2 with the pseudo components are altered from 0.10 to 0.15, the AAD is reduced to 7.6% for Feed #4 and to 0.4% for Feed #5.

Li et al. (2013b) presented *P–T* conditions for three-phase behavior for the mixture of 83.2% CO_2, 11.8% n-C_4, and 34.3% heavy oil 4 on the molar basis (Feed #15 in Li et al., 2013b). Fig. 13 compares the predicted phase boundaries with the data points given in Li et al. (2013b). Although the lower pressure boundary is overestimated, the higher pressure boundary is predicted quite accurately with no further adjustment of the fluid model from the direct PnA algorithm.

5. Discussion

The direct PnA method is simpler than the previous PnA method (Kumar and Okuno, 2013), but exhibits equivalent or improved predictive capability. For example, the previous PnA method resulted in an AAD of 6.7% in MMP calculation for 8 fluids tested in Kumar and Okuno (2013), which is higher than the AAD of 6.4% obtained for MMPs of the cases given in Tables 1 and 2 (see Section 4.1). The AAD for CVD liquid saturation for 34 gas condensates (data type 1 in Table 3) was 1.06% using the direct PnA method, but it was 1.8% for 27 gas condensates tested in Kumar and Okuno (2013). The AAD for CVD liquid saturation for volatile oils calculated with the direct PnA method was 2.7% (data type 1 in Table 4), but it was 3.7% for 4 fluids tested in Kumar and Okuno (2013). The oleic phase saturations calculated for the swelling test for the West Sak heavy oil showed the AAD of 3.6% with the direct PnA method (see Table 5) and 4.1% with the previous PnA method (Kumar and Okuno, 2013). In the preceding section, the improved predictions with the direct PnA method were also shown in comparison with CM_wV (Figs. 6–11).

In this section, a few fundamental aspects of the direct PnA method are discussed. Section 5.1 discusses systematic control of phase behavior predictions through Eq. (7). Section 5.2 presents the advantage of the optimized critical parameters (Eqs. (S8)–(S10)) over estimated physical critical parameters for *n*-alkanes in reservoir fluid characterization. Section 5.3 discusses adjustment of BIPs with the direct PnA method.

5.1. Systematic control of phase behavior predictions

The unique feature of the direct PnA method is that it systematically controls phase behavior predictions through three key parameters. As discussed in Section 3, f_b is able to monotonically change volumetric phase behavior predictions from the PR EOS through Eq. (3). The ψ parameter as a linear function of MW is adjusted by g and C in Eq. (7), which controls compositional phase behavior predictions. These three key parameters, f_b, g, and C, are not component-specific, and applied to all pseudo components for the fluid of interest. This is the fundamental reason for the systematic control of phase behavior predictions in the direct PnA method.

Table 4
Converged f_ψ, f_b, and p values for volatile oils characterized using the direct PnA method. CVD or CCE data are available for these oils.

Oil nos.	References	MW (g/mol)	°API	Res. temp. (K)	f_ψ	f_b	p	Data limits value (type[#])	Dev.[¥]
1	Al-Meshari (2004), Fluid-12	46.07	50.3	354.82	0.8544	+0.033[x]	2.3	38.20 (1)	2.80
2	Al-Meshari (2004), Fluid-13	56.06	36.7	364.82	0.2188	0.1091	2.3	3.93 (3)	0.02
3	Al-Meshari (2004), Fluid-14	54.57	40.7	360.93	0.3069	0.1081	2.4	1.00 (3)	0.01
4	Al-Meshari (2004), Fluid-15	51.11	57.5	353.15	1.5275	0.0581	2.9	2.98 (3)	0.01
5	Al-Meshari (2004), Fluid-16	59.63	55.6	425.93	0.0591	−0.006[x]	2.5	35.30 (1)	2.29
6	Al-Meshari (2004), Fluid-17	67.32	44.5	414.82	0.2061	0.0920	2.5	6.84 (3)	0.04
7	Al-Meshari (2004), Fluid-18	59.90	54.4	423.15	0.2876	0.0591	3.2	7.57 (3)	0.04
8	Al-Meshari (2004), Fluid-19	62.65	59.5	377.59	1.2666	0.0540	4.3	4.08 (3)	0.00
9	Oil[*]	86.68	56.6	376.75	1.7416	0.0360	4.0	2.46 (3)	0.01
10[ǂ]	McVay (1994), Oil A	50.93	44.5	408.70	1.1997	+0.000[x]	2.5	33.30 (1)	4.38
11	McVay (1994), Oil B	57.50	56.7	393.70	1.0877	+0.000[x]	3.1	49.50 (1)	2.60
12[ǂ]	Yang et al. (1997)[ǂ]	37.94	57.5	371.60	−0.6776	+0.085[x]	2.0	6.06 (2)	2.12
13	Jacoby and Yarborough (1967)	54.32	63.7	346.48	1.1580	0.0540	2.8	24.29 (1)	1.60
14[ǂ]	Pedersen et al. (1988)	47.84	52.5	424.25	0.2597	−0.013[x]	2.3	42.20 (1)	3.87
15	Reudelhuber and Hinds (1956)	42.55	49.1	374.82	0.6933	−0.024[x]	2.3	34.50 (1)	1.60

ǂ As reported. All other API gravities are calculated from density at 288.15 K and 1.01325 bar.
ǂ Near critical volatile oil.
[x] Δc value (f_b is zero).
[#] (1) is CVD liquid saturation (%), (2) is CCE liquid saturation (%), and (3) is CCE relative volume.
[¥] Deviation is the summation of |experimental value −predicted value| divided by the number of data points.
[*] Data source is not mentioned for confidentiality.

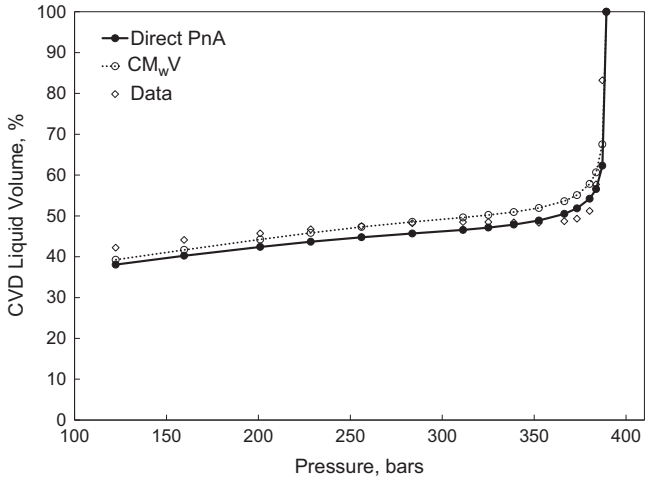

Fig. 8. Comparison between the measured and predicted CVD liquid saturations for near-critical volatile oil 14 in Table 4 at 424.25 K (Pedersen et al., 1988). The critical point was measured at 426 K and 388 bar, but it is calculated to be 433.00 K and 389.95 bar by the fluid model based on the direct PnA method. Although the calculated T_C is 7 K higher than the measured T_C, the CVD liquid saturations are accurately predicted.

In the algorithm presented in the current paper, a mechanism was developed for adjustment of g and C through f_ψ for a given f_b, or for a given c in characterization of light fluids for which f_b is zero. However, it is also possible to control compositional phase behavior predictions by adjusting C, which uniquely gives a corresponding value for g through the constraint $\varepsilon < \varepsilon_{TOL}$; matching of P_{SAT} for the fluid of interest. This is useful to match other phase behavior data, such as CVD liquid saturations and MMPs.

Fig. 14 presents CVD liquid saturations predicted with different values for C for gas condensate 6 in Table 3. Note that C is equal to c for this fluid because f_b is zero. A monotonic variation of the CVD liquid saturation curve with the C parameter is evident in the figure. An optimum value for C, which is 0.91 in this case, is easy to find because of the monotonic, systematic change of the CVD liquid saturation curve.

Fig. 15 shows MMPs calculated with different C values for oil 1 in Table 1. The calculated MMP decreases monotonically with decreasing C. It is not difficult to find the value for C with which the measured MMP is matched.

5.2. Phase behavior predictions in composition space with optimized critical parameters

In the PnA methods of Kumar and Okuno (2013) and in this research, the initializations of the attraction and covolume parameters are based on the T_C, P_C, and m parameters optimized for n-alkanes by use of the PR EOS (Eqs. (S8)–(S10)). The differences from physical critical parameters estimated by Constantinou and Gani (1994) were discussed in the Supporting information (Part 1). In general, the optimized critical parameters tend to be higher than estimated physical values for n-alkanes; e.g., the sets of critical parameters from Constantinou and Gani (1994) and Gao et al. (2001). The higher critical parameters result in extended two-phase lines in P–T space for pure components. To show the effect of the higher critical parameters on phase behavior predictions in composition space, Kumar and Okuno (2012) compared bubble- and dew-point predictions for n-alkane binaries by using two sets of critical parameters; i.e., the optimized parameters from Kumar and Okuno (2012) and the estimated physical parameters from Gao et al. (2001). BIPs were set to zero for systematic comparisons. Predictions of bubble- and dew-points for nine n-alkane binaries were closer to experimentally measured data points when the optimized parameters were used. It was also shown that critical points of three n-alkane binaries (n-C_6 with n-C_{16}, n-C_{24}, and n-C_{36}) were more accurately predicted by use of the optimized parameter set.

This subsection gives further comparisons of phase behavior predictions for more than two components by using the optimized parameters of Kumar and Okuno (2012) and the physical parameter estimated by Constantinou and Gani (1994). For both cases, BIPs for hydrocarbon pairs are set to zero for systematic comparisons. Fig. 16 presents the two-phase envelopes predicted with the two sets of critical parameters for an n-alkane mixture consisting of 44.0% C_1, 45.8% n-C_{10}, 6.8% n-C_{18}, and 3.4% n-C_{30}. The bubble-point data were taken from Daridon et al. (1996). The two-phase envelope is predicted to be greater in P–T space when the optimized parameters are used. This is in line with the comparisons made for n-alkane binaries in Kumar and Okuno (2012). The PR EOS with the optimized critical parameters gives more accurate

Table 5
Converged f_ψ, f_b, and p values for heavy oils characterized using the direct PnA method. PVT data available for these oils include swelling tests, gas solubility, and phase envelopes.

Oil nos.	References	MW (g/mol)	°API	Res. temp. (K)	No. of density data	f_ψ	f_b	p	AAD%	Type of data
1	Sharma (1990), West Sak oil	228.88	18.68	299.81	10	0.0568	0.1491	5.7	3.62	Swelling Test
2	Krejbjerg and Pedersen (2006), Fluid-1	125.72	28.00‡	347.15	13	0.2762	0.2341	5.5	3.40	Swelling Test
3	Pedersen et al. (2004), Fluid-22	311.06	10.87	305.45	11	−0.0607	0.1592	5.5	3.13	GOR
4	Li et al. (2013a), Lloydminster oil	482.00	10.80	294.15	1	−0.3409	0.1320	9.0	9.30	Swelling Test

‡ As reported. All other API gravities are calculated from density at 288.15 K and 1.01325 bar.

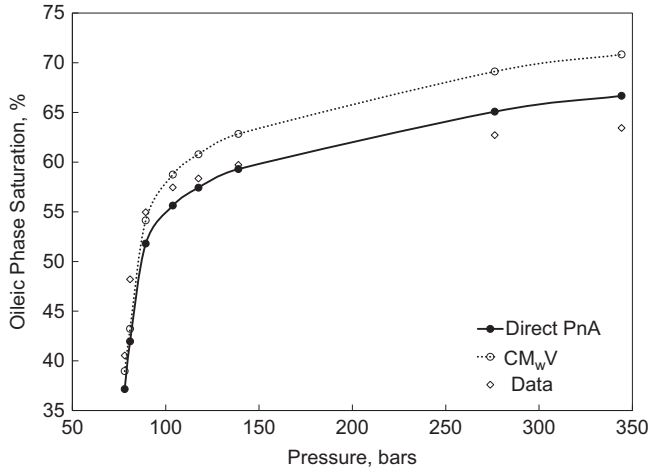

Fig. 9. Oleic phase saturation data and predictions for heavy oil 1 (Sharma, 1990) given in Table 5 at 299.81 K. This is a mixture of 20% oil and 80% CO_2. The AAD for these oleic phase saturation calculations is 5.2% with the direct PnA method.

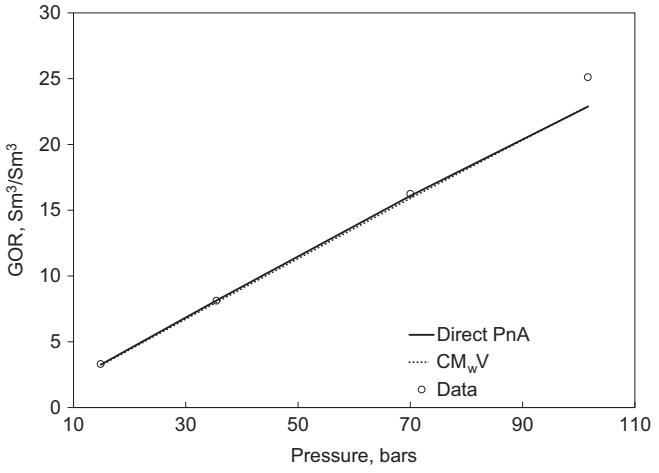

Fig. 11. Data and predictions for the gas–oil-ratios (GOR) for heavy oil 3 (Pedersen et al., 2004) at the reservoir temperature of 305.45 K. The AAD of the GOR predictions is 2.9% with the direct PnA method.

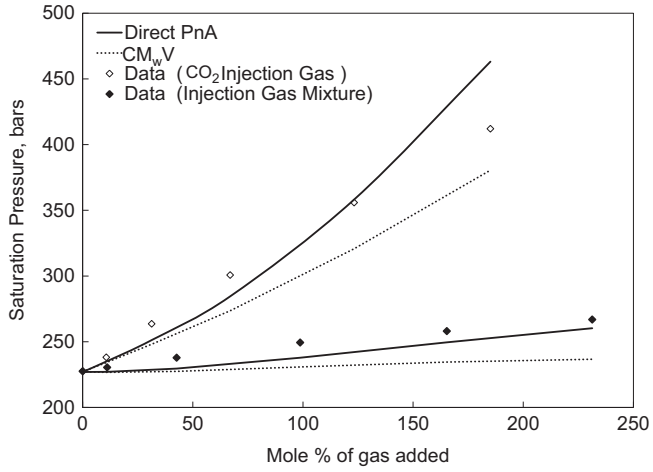

Fig. 10. Data and predictions for saturation pressures in the swelling tests of heavy oil 2 with two injection gases; CO_2 and a light gas mixture (Krejbjerg and Pedersen, 2006). The AAD is 3.9% for the CO_2 case and 2.8% for the gas mixture case with the direct PnA method.

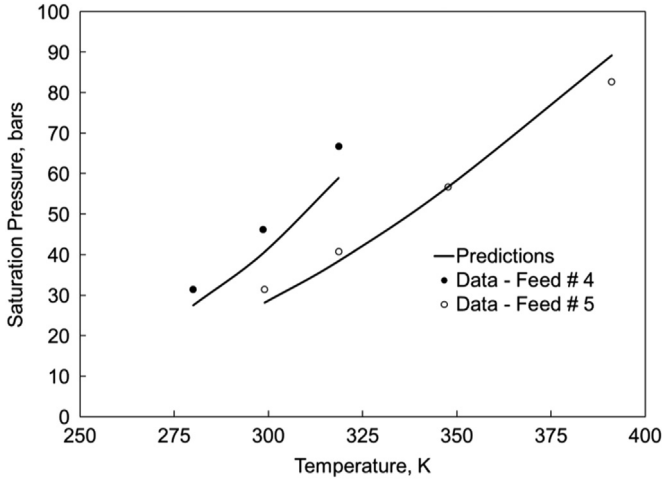

Fig. 12. Saturation pressures measured and predicted for two mixtures with the Lloydminster heavy oil (heavy oil 4 in Table 5), Feeds #4 and #5 in Li et al. (2013a). The AAD of the saturation pressure predictions is 13.7% for Feed #4 and 6.0% for Feed #5. If the BIPs for CO_2 with the pseudo components are altered from 0.10 to 0.15, the AAD is reduced to 7.6% for Feed #4 and to 0.4% for Feed #5.

predictions in composition space than with the estimated physical critical parameters.

Fig. 17 shows saturation pressure predictions in a swelling test for a 25-component oil with a gas at 373.15 K presented in Danesh et al. (1991). The oil consists of 90.68% *n*-alkanes from C_1 through n-C_{20}, 0.72% toluene, 1.79% xylene, 2.20% cyclo-hexane, 2.25% methyl-cyclo-pentane, and 2.36% methyl-cyclo-hexane. The injection gas consists of 69.82% C_1, 13.09% C_2, 11.10% C_3, and 5.99% n-C_4. The AAD of the saturation pressure predictions is 11% when the physical parameter set is used, whereas it is 4% with the optimized parameter set.

Fig. 18 depicts the two-phase envelopes predicted in composition space for a ternary system of CO_2, C_3, and n-C_{20} at 338.65 K and 69.92 bar. Experimental data were taken from Al-Marri (2006). As recommended by Peng and Robinson (1978), 0.10 is used for the BIPs of CO_2 with the *n*-alkanes. The optimized parameter set results in more accurate predictions of two-phase equilibrium for the *n*-alkane mixtures containing CO_2. When the CO_2 BIPs are set to 0.0, the two-phase region is predicted to be smaller in composition space.

The results presented in this subsection show that the PR EOS gives reasonably accurate predictions for *n*-alkane mixtures even with zero BIPs when the optimized set of critical parameters is used. When non-zero BIPs are required for CO_2-*n*-alkane mixtures, req-

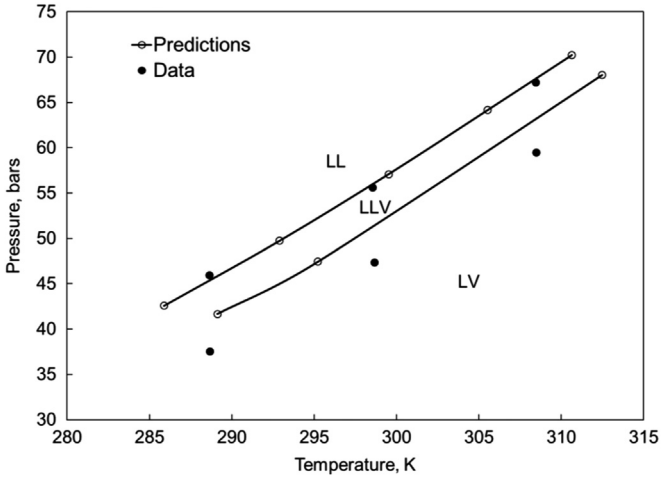

Fig. 13. The three-phase boundaries measured and predicted for a mixture of heavy oil 4 (Table 5) with CO_2 and n-C_4 (Feed #15 of Li et al., 2013b).

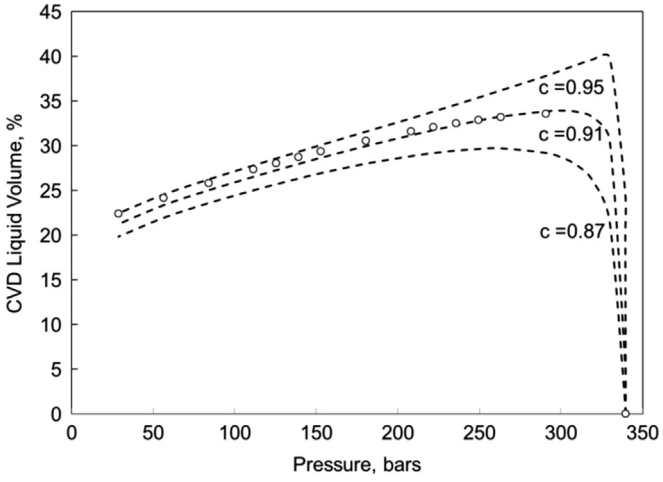

Fig. 14. CVD liquid saturations predicted with different values for C for gas condensate 6 in Table 3. C is equal to c for this fluid because f_b is zero. An optimum value for C, which is 0.91 in this case, is easy to find because of the monotonic, systematic change of the CVD liquid saturation curve.

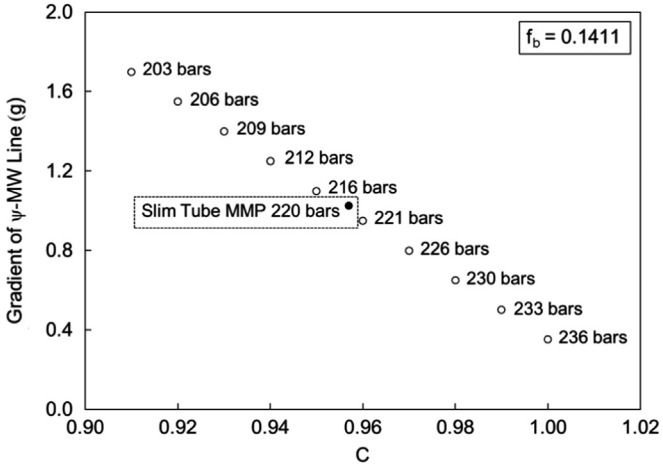

Fig. 15. MMPs calculated with different C values for oil 1 given in Table 1. The calculated MMP decreases monotonically with decreasing C. It is not difficult to find the value for C with which the measured MMP is matched.

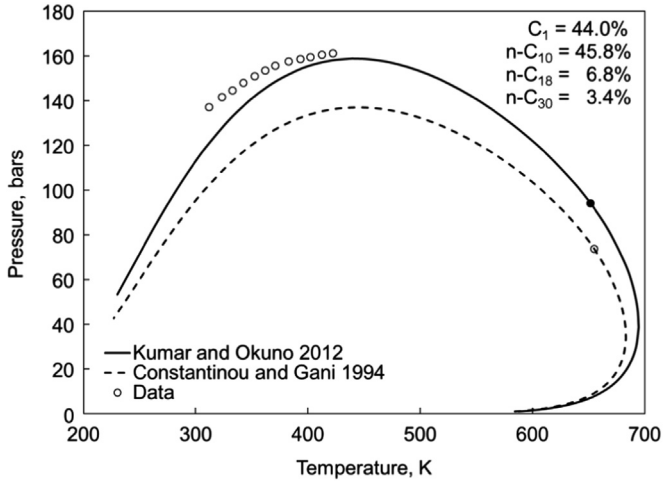

Fig. 16. Two-phase envelopes predicted with the two sets of critical parameters for an n-alkane mixture consisting of 44.0% C_1, 45.8% n-C_{10}, 6.8% n-C_{18}, and 3.4% n-C_{30}. The optimized critical parameters of Kumar and Okuno (2012) and the estimated physical critical parameters of Constantinou and Gani (1994) are used with the PR EOS. The BIPs are zero for both cases. The bubble-point data were taken from Daridon et al. (1996). Use of the optimized critical parameters results in a more accurate P–T envelope.

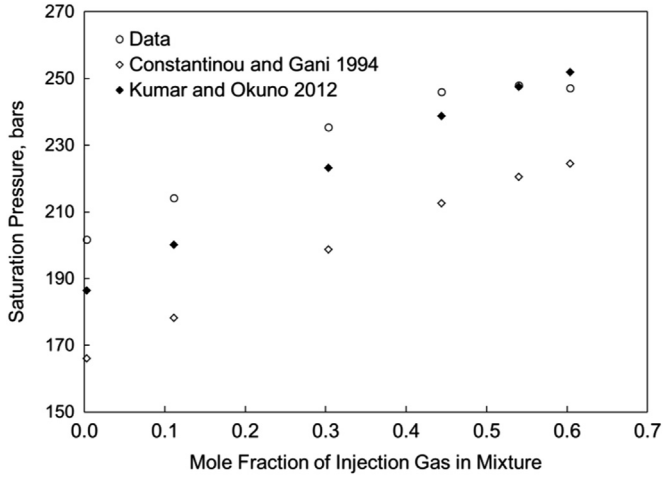

Fig. 17. Saturation pressures measured and predicted for a 25-component oil with a gas at 373.15 K presented in Danesh et al. (1991). The AAD of the saturation pressure predictions is 11% when the physical parameter set (Constantinou and Gani, 1994) is used, whereas it is 4% with the optimized parameter set (Kumar and Okuno, 2012). The BIPs are zero for both sets of predictions.

uired deviations from zero are smaller with the optimized critical parameters than with estimated physical critical parameters. However, these results are limited by the availability of experimental data. Note that the optimized critical parameters were developed for use in reservoir fluid characterization, as described in this paper and Kumar and Okuno (2012, 2013). If they were used for pure n-alkanes with the PR EOS, the altered critical points would give extended vapor–pressure curves for heavy n-alkanes, as shown in Fig. S1.

5.3. Adjustment of BIPs

The extensive testing of the PnA methods of Kumar and Okuno (2013) and in this research has indicated that the PR EOS gives satisfactory predictions of reservoir fluid phase behavior with zero BIPs for all hydrocarbon pairs. Recommended values have been used for non-hydrocarbon components, such as N_2 and CO_2, as constants (Peng and Robinson, 1978). However, these default BIPs

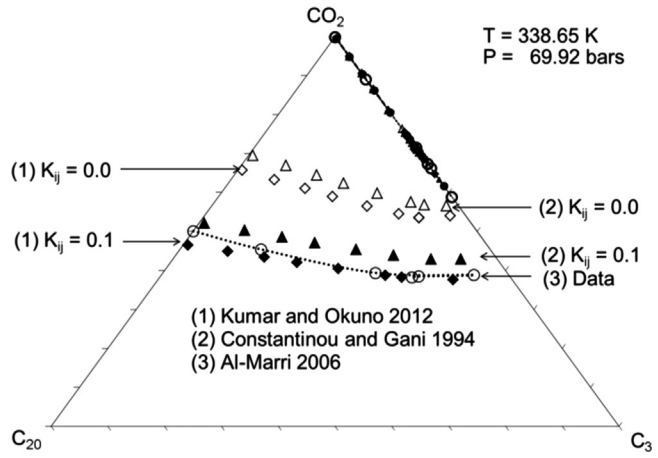

Fig. 18. Two-phase envelopes predicted for a ternary system of CO_2, C_3, and n-C_{20} at 338.65 K and 69.92 bar using the PR EOS with the critical parameters from Kumar and Okuno (2012a) and Constantinou and Gani (1994). The BIPs considered for CO_2 with the other two components are 0.0 and 0.1. Peng and Robinson (1978) recommended 0.1 for these BIPs. The optimized parameter set results in more accurate predictions of two-phase equilibrium for the *n*-alkane mixtures containing CO_2. The data were taken from Al-Marri (2006).

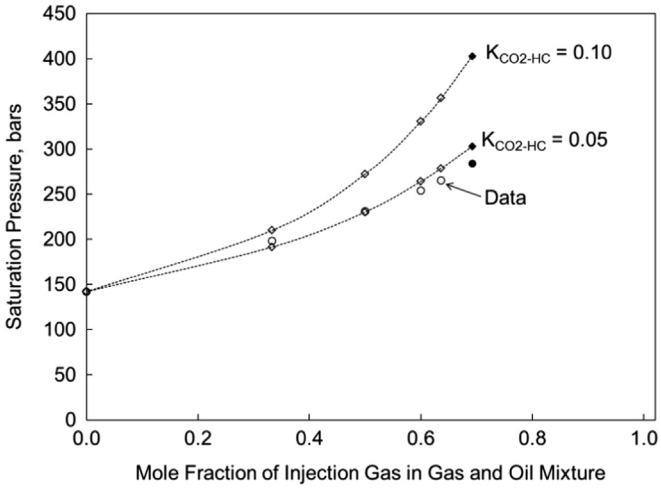

Fig. 19. Saturation pressures measured in the swelling test of Fluid 18 (Table 1) with CO_2 at 394 K (Negahban et al., 2010). The experimental MMP for this oil with CO_2 is 178 ± 2 bar at 394 K. The fluid model developed based on the direct PnA method gives an MMP of 188 bar with the default BIPs of CO_2 with pseudo components as 0.10. Although it correctly predicts the transition from bubble- to dew-point at CO_2 concentration of 0.69, this fluid model gives progressively higher saturation pressures than the experimental values with increasing CO_2 concentration. When the BIPs of CO_2 with pseudo components are reduced from 0.10 to 0.05, the model is much improved in saturation pressure predictions. The MMP predicted is 174 bar, which is still close to the experimental result. The blank and filled markers represent bubble- and dew-points, respectively.

may be adjusted especially for non-hydrocarbon components with pseudo components.

Fig. 19 shows saturation pressures measured in the swelling test of Fluid 18 (Table 1) with CO_2 at 394 K (Negahban et al., 2010). The experimental MMP for this oil with CO_2 is 178 ± 2 bar at 394 K. The fluid model developed based on the direct PnA method gives an MMP of 188 bar with the default BIPs of CO_2 with pseudo components as 0.10. Although it correctly predicts the transition from bubble- to dew-point at CO_2 concentration of 0.69, this fluid model gives progressively higher saturation pressures than the experimental values with increasing CO_2 concentration. When the BIPs of CO_2 with pseudo components are reduced from 0.10 to 0.05, the model is much improved in saturation pressure predictions as shown in Fig. 19. The MMP predicted is 174 bar, which is still close to the experimental result.

6. Conclusions

A new method was developed for reservoir fluid characterization that directly perturbs the attraction and covolume parameters of pseudo components from *n*-alkanes' values (direct perturbation from *n*-alkanes, or direct PnA). The direct PnA method was successfully applied to 84 different reservoir fluids, such as gas condensates, volatile oils, black oils, and heavy oils. The regression algorithm used only the P_{SAT} at T_{RES} and liquid densities at T_{RES} at different pressures for each fluid. Other available data, such as MMPs, liquid saturations in CVD and CCE, and gas solubilities, were used to test the predictive capability of the fluid models developed by the direct PnA method. The PR EOS with the vdW mixing rules was used throughout this research. Conclusions are as follows:

- The reservoir fluids tested were reliably characterized by systematic adjustment of the attraction and covolume parameters of pseudo components. The covolume parameters were perturbed from *n*-alkane values by f_b in Eq. (3). The f_b parameter monotonically changes volumetric phase behavior predictions. As in our previous research, the $\psi(=a/b^2)$ parameter was used to ensure proper interrelationship between the attraction (a) and covolume (b) parameters. A new approach to adjustment of the ψ parameters was developed with a linear ψ function of MW. The g and C parameters in Eq. (7) control compositional phase behavior predictions in a regular manner in the regression algorithm presented.
- The three key parameters, f_b, g, and C, are not component-specific, and applied to all pseudo components for the fluid of interest. This enables to control phase behavior predictions in a systematic, monotonic manner in the direct PnA method. The direct PnA method does not require estimation or extrapolation for apparent critical parameters of heavy fractions, which are mixtures of non-identifiable compounds.
- The direct PnA method substantially simplifies the characterization of reservoir fluids by use of the PR EOS. The simplification was possible because of the inherent accuracy and simplicity of the PR EOS and the adjustment parameters found in this research. The regression process of the PnA method requires only a few seconds per fluid using a personal computer.
- One of the important data types required for the direct PnA method is liquid densities that capture the level of aromaticity in the fluid system of interest. Results indicated that densities of equilibrium liquid phases in a multiphase region are more effective than densities in a single-phase region for capturing the level of aromaticity in the PnA method.
- No change is required for the functional form of the EOS and mixing rules. The method can be readily implemented in existing software based on the PR EOS with the vdW mixing rules.

Nomenclature

Roman symbols

a	attraction parameter defined in Eq. (S2)
a_c	attraction parameter at a critical temperature defined in Eq. (S3)
α	temperature dependent parameter defined in Eq. (S4)

A	aromatics
b	covolume parameter defined in Eq. (S5)
c	parameter defined in Eq. (5)
c'	parameter defined in Eq. (6)
C	$c+c'$
f_ψ	perturbation factor for the ψ parameters
f_b	perturbation factor for the covolume parameters
f_m	perturbation factor for the m parameters in Eq. (S10)
f_P	perturbation factor for P_C in Eq. (S9)
f_T	perturbation factor for T_C in Eq. (S8)
m_{bi}	parameter defined with Eq. (3)
g	slope of the ψ parameter in MW space
m	parameter defined in Eqs. (S6) and (S7)
M_r	molecular weight of the lightest pseudo component divided by 100.20
n	number of pseudo components
N	napthenes
e_i	objective function for the ith pseudo component defined in Eq. (B-4)
p	pressure (bar)
P	paraffins
P_C	critical pressure (bar)

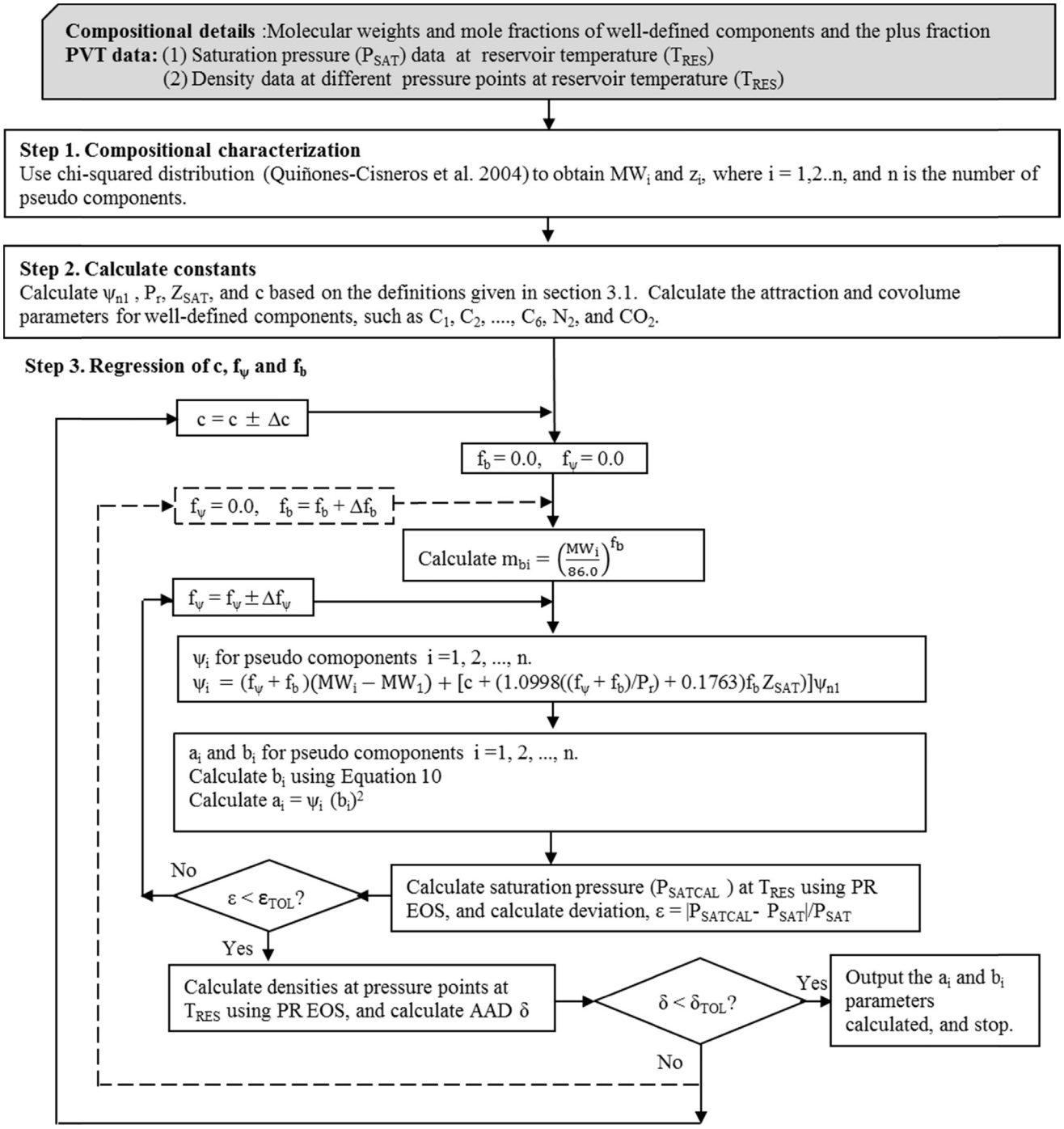

Fig. A1. Flow chart for the direct perturbation algorithm presented in Section 3. The dotted line shows the adjustment of f_b for matching densities. This path is taken when the adjustment of c is unsuccessful in matching densities (see Section 3.2 for details). For the dotted path, the c value calculated in Step 2 is used and kept constant during the regression with f_b and f_ψ.

P_r ratio of the saturation pressure calculated as n-alkanes to P_{SAT}
P_{SAT} experimental saturation pressure at reservoir temperature
P_{SATCAL} calculated saturation pressure
P_{vap} vapor pressure
R universal gas constant
S parameter in the chi-squared distribution function given in Eq. (S11)
T temperature (K)
T_b boiling point temperature (K)
T_C critical temperature (K)
T_r T in Kelvin divided by 277.0
T_{RES} reservoir temperature
v molar volume (g/mol) (Eq. (S1))
V_C critical volume (g/mol)
Y_a aromaticity as defined by Yarborough (1979)
Z_{SAT} liquid compressibility factor at the saturation pressure at T_{RES}

Greek symbols

ε absolute average deviation for saturation pressure calculations
δ deviation for density calculations
γ standard specific gravity
Γ gamma function
ρ_L^S saturated liquid density
ρ_{SAT} density at saturation pressure
Ω_a constant term (=0.45723552892138219) in the attraction parameter of the PR EOS
Ω_b constant term (=0.0777960739038884574) in the covolume parameter of the PR EOS
ψ parameter given by Eq. (1)
ψ_{n1} normal-alkane equivalent ψ for the lightest pseudo component
ω acentric factor

Abbreviations

°API API (American Petroleum Institute) gravity (=141.5/γ − 131.5)
AAD average absolute deviation
AD average deviation
BIP binary interaction parameter
CM_wV conventional fluid characterization method with volume shifting (Pedersen and Christensen, 2007)
CN carbon number
CVD constant volume depletion
CCE constant composition expansion
CP critical point
EOS equation of state
GOR gas oil ratio
LL liquid–liquid
LLV liquid–liquid–vapor
LV liquid–vapor
MMP minimum miscibility pressure (bar)
MW molecular weight (g/mol)
MW_{avg} average molecular weight
PC pseudo component
PnA perturbation from n-alkanes
PR Peng–Robinson
P–T pressure–temperature
SCN single carbon number fraction
SRK Soave–Redlich–Kwong
Tol. tolerance
vdW van der Waals

Subscripts

i index for pseudo components
j index for the iteration loop for matching the saturation pressure by adjusting f_ψ
k index for the iteration loop for mating densities by adjusting f_b

Acknowledgements

This research was funded by the Natural Sciences and Engineering Research Council of Canada (RGPIN 418266) and Japan Petroleum Exploration Co., Ltd. Ashutosh Kumar was awarded the Union Pacific Resources Inc. Graduate Scholarship in Petroleum Engineering at the University of Alberta. Ryosuke Okuno was awarded the SPE Petroleum Engineering Junior Faculty Research Initiation Fellowship 2012–2013. We gratefully acknowledge these supports. We also thank Dr. Russell T. Johns for providing the PennPVT software.

Appendix A. Algorithm for direct perturbation of attraction and covolume parameters

See Fig. A1.

Appendix B. Estimation of critical parameters from attraction and covolume parameters

The attraction and covolume parameters cannot be directly input for the fluid model used in existing commercial software, such as numerical reservoir and PVT simulators. Mathematically, any set of T_C, P_C, and m (or ω) that results in a given set of the attraction and covolume parameters will yield the same phase behavior prediction from the PR EOS fluid model at a given temperature. However, attaining a qualitative and quantitative correctness may be important when such parameters are used for calculation of some other properties, such as parachor values,

Table B1
Example of solution for T_C, P_C, and ω from the attraction and covolume parameters using the EXCEL solver. The temperature is 299.81 K.

Target a_i (bar/cm^2/mol^2)	Target b_i (cm^3/mol)	γ_i	T_{bi} (K)	T_{Ci}[a] (K)	P_{Ci}[a](bar)	ω_i[a]	e_i
152,780,160.65	225.96109	0.82984	517.749	700.347	20.049	0.5680	3.64E−07
415,755,584.46	371.98724	0.94476	670.127	853.779	14.847	0.8738	2.83E−06
809,603,339.61	518.89867	1.04283	797.501	982.191	12.244	1.0646	1.79E−06
1893,146,362.73	796.38678	1.21313	1006.301	1199.746	9.745	1.2633	9.37E−06

[a] T_{Ci}, P_{Ci}, and ω_i are calculated using the correlations of Kesler-Lee (1976) and Lee-Kesler (1975) with the listed γ_i and T_{bi}. The target a_i and b_i values are sample values for the attraction and covolume parameters for pseudo component i. Four pseudo components are listed.

interfacial tensions, and critical viscosities. A method is presented to back calculate a physically reasonable set of T_C, P_C, and ω that gives a certain set of the attraction and covolume parameters converged by the direct PnA algorithm (Section 3).

The correlations of Kesler-Lee (1976) and Lee-Kesler (1975) are widely used to estimate of T_C, P_C, and ω of petroleum fractions (Whitson and Brulè, 2000). They are functions of boiling point (T_b) and specific gravity (γ). Thus, for pseudo component i, the method proposed is to find a set of T_{bi} and γ_i that gives the desired values of the attraction (a_i) and covolume (b_i) parameters through the correlations of Kesler-Lee (1976) and Lee-Kesler (1975).

To give reasonable initial values for T_{bi} and γ_i, a model is proposed for T_{Ci} by replacing f_T of Eq. (S8) with m_{bi} used in Eq. 3. Then, Eq. (S5) is solved for P_{Ci} for a given T_{Ci} and b_i. After that, m_i can be solved for using Eqs. (S2)–(S4) for a given T_{Ci}, P_{Ci}, and a_i. The resulting T_{Ci}, P_{Ci}, and m_i are used with the PR EOS to give initial values for T_{bi} and γ_i.

A step-wise description of the method is as follows:

Step 1. Calculate T_{Ci}, P_{Ci}, and m_i by use of the following equations:

$$T_{Ci} = 1154.35 - 844.83\left(1.0 + 1.7557 \times 10^{-3} m_{bi} M_{Wi}\right)^{-2.0} \quad (B-1)$$

$$P_{Ci} = \frac{\Omega_b R T_{Ci}}{b_i} \quad (B-2)$$

$$m_i = \left[\sqrt{\frac{a_i}{\Omega_a (RT_{Ci})^2 / P_{Ci}}} - 1.0\right] \Big/ \left(1.0 - \sqrt{\frac{T}{T_{Ci}}}\right). \quad (B-3)$$

Step 2. Calculate T_{bi} and γ_i using the PR EOS with the T_{Ci}, P_{Ci}, and m_i from step 1.Step 3. Calculate T_{Ci}, P_{Ci}, and ω_i using the correlations of Kesler-Lee (1976) and Lee-Kesler (1975) with the T_{bi} and γ_i from step 2.Step 4. Calculate a_i' and b_i' for the PR EOS using Eqs. (S2) and (S5) with the T_{Ci}, P_{Ci}, and ω_i from step 3. Step 5. Calculate the objective function (e_i) for pseudo component i as follows:

$$e_i = |a_i - a_i'|/a_i + |b_i - b_i'|/b_i \quad (B-4)$$

If e_i is less than a tolerance, repeat the method for other pseudo components. Otherwise, update T_{bi} and γ_i to reduce e_i until it becomes less than the tolerance. In the current research, the EXCEL solver was used to perform the iterations. Table B1 gives the results for four pseudo components in a sample calculation.

Appendix C. Supporting information

Supplementary data associated with this article can be found in the online version at http://dx.doi.org/10.1016/j.ces.2015.01.032.

References

Ahmadi, K., Johns, R.T., 2011. Multiple mixing-cell model for MMP determination. Soc. Petrol. Eng. J. 16, 733–742.

Ahmed, T., Meehan, D. N., 2010. A practical approach for calculating EOS coefficients. In: Presented at SPE Russian Oil & Gas Technical Conference and Exhibition held in Moscow, Russia, 26–28 October 2010.

Al-Ajmi, M.F., Tybjerg, P., Rasmussen, C.P., Azeem, J., 2011. EOS Modeling of two major Kuwaiti oil reservoirs. In: Paper SPE 141241 Presented at SPE Middle East Oil and Gas Show and Conference, Manama, Bahrain, 25–28 September.

Al-Marri, S.S., 2006. PVT, Phase Behavior and Viscosity Measurements and Modeling of the Ternary and Binary Systems of Carbon Dioxide +Heavy Hydrocarbon (*n*-Eicosane)+Light Gas (Ethane or Propane) (Ph.D. Dissertation). University of Southern California, USA.

Al-Meshari, A., 2004. New Strategic Method to Tune Equation of State to Match Experimental Data for Compositional Simulation (Ph.D. Dissertation). Texas A&M University, TX. USA.

Al-Subai, K.O., 2001. Compositional Gradient Calculations for a Saudi Arabian Gas Condensate Reservoir (M.Sc. Thesis). King Fahd University of Petroleum & Minerals, Saudi Arabia.

Aparicio-Martínez, S., Hall, K.R., 2006. Phase equilibria in water containing binary systems from molecular based equation of state. Fluid Phase Equilib. 254, 112–125.

Clark, P., Toulekima, S., Sarma, H., 2008. In: Presented at SPE Asia Pacific Oil and Gas Conference and Exhibition, October 20–22, 2008. Perth, Australia.

Coats, K.H., 1985. Simulation of gas condensate reservoir performance. J. Pet. Technol. 37, 1870–1886.

Coats, K.H., Smart, G.T., 1986. Application of a regression based eos PVT program to laboratory data. SPE Reservoir Eng. 1, 277–299.

Constantinou, L., Gani, R., 1994. New group contribution method for the estimating properties of pure compounds. AIChE J. 40, 1697–1710.

Danesh, A., 1998. PVT and Phase Behavior of Petroleum Reservoir Fluids. Elsevier Science & Technology Books p. 1998.

Danesh, A., Xu, D.-H., Todd, A.C., 1991. Comparative study of cubic equation of state for predictive phase behavior and volumetric properties of injection gas-reservoir oil systems. Fluid Phase Equilib. 63, 259–278.

Daridon, J.L., Xans, P., Montel, F., 1996. Phase boundary measurement on a methane+decane+multiparaffins system. Fluid Phase Equilib. 117, 241–248.

Drohm, J.K., Trengove, R.D., Goldthrope, W.H., 1988. On the quality of data from standard gas-condensate PVT experiments. In: Presented at the SPE Gas Technology Symposium, Dallas, Texas, 13–15 June.

Economou, I.G., Heidman, J.L., Tsonopoulos, C., Wilson, G.M., 1997. Mutual solubilities of hydrocarbons and water: III. 1-Hexene, 1-octene, C_{10}–C_{12} hydrocarbons. AIChE J. 43, 535–546.

Egwuenu, A.M., Johns, R.T., Li, Y., 2008. Improved fluid characterization for miscible gas floods. SPE Reservoir Eval. Eng. 11, 655–665.

Ekundayo, J.M., 2012. Configuration of Slim Tube Apparatus for Consistent Determination of Minimum Miscibility Pressure (MMP) Data (M.Sc. Thesis). The Petroleum Institute, Abu Dhabi, UAE.

Enick, R.M., Holder, G.D., Mohamed, R., 1987. Four-phase flash equilibrium calculations using the Peng–Robinson equation of state and a mixing rule for asymmetric systems. SPE Reservoir Eng. 2, 687–694.

Fawumi, O.K., 1999. Effect of Liquid Drop-out on the Productivity of a Rich Gas Condensate Reservoir (M.Sc. Thesis). King Fahd University of Petroleum & Minerals, Saudi Arabia.

Gao, W., Robinson Jr., R.L., Gasem, K.A.M., 2001. Improved correlations for heavy *n*-paraffin physical properties. Fluid Phase Equilib. 179, 207–216.

Graue, D.J., Zana, E.T., 1981. Study of a possible CO_2 flood in Rangely field. J. Pet. Technol. 33, 1312–1318.

Guo, T.M., Du, L., 1989. A New Three-Parameter Cubic Equation of State for Reservoir Fluids. , Parts-III Application to Gas Condensates, SPE 19374-MS.

Heidman, J.L., Tsonopoulos, C., Bardy, C.J., Wilson, G.M., 1985. High-temperature mutual solubilities of hydrocarbons and water. AIChE J. 31, 376–384.

Hosein, R., Jagai, T., Dawe, R.A., 2013. A method for predicting the phase behaviour of trinidad gas condensates. WIJE 35, 22–30.

Høier, L., 1997. Miscibility Variation in Compositional Grading (Ph.D. Dissertation). Norwegian University of Science and Technology, Norway.

Ikeda, M., Schaefer, L., 2011. Examining the effect of binary interaction parameters on vle modelling using cubic equations of state. Fluid Phase Equilib. 305, 233–237.

Imo-Jack, O. 2010. PVT characterization of a gas condensate reservoir and investigation of factors affecting deliverability. In: Presented at Annual SPE International Conference and Exhibition, Tinapa-Calabar, Nigeria, 31 July–7 August.

Jacoby, R.H., Yarborough, L., 1967. Reservoir fluids and their uses. Appl. Thermodyn. Symp. 59, 49–62.

Jacoby, R.H., Koeller, R.C., Berry Jr., V.J., 1959. Effect of composition and temperature on phase behavior and depletion performance of rich gas-condensate systems. Trans. AIME 216, 406–411.

Jaubert, J.-N., Avaullee, L., Souvay, J.-F., 2002. A crude oil data bank containing more than 5000 PVT and gas injection data. J. Pet. Sci. Technol. 34, 65–107.

Kesler, M.G., Lee, B.I., 1976. Improve prediction of enthalpy of fractions. Hydrocarbon Process. 55, 153–158.

Kilgren, K.H., 1966. Phase behavior of a high-pressure condensate reservoir fluid. J. Pet. Technol. 18, 1001–1005.

Krejbjerg, K., Pedersen, K.S., 2006. Controlling VLLE equilibrium with a cubic EoS in heavy oil modeling. In: 57th Annual Technical Meeting of the Petroleum Society (Canadian International Petroleum Conference), Calgary, Canada, 13–15 June 2006.

Kumar, A., Okuno, R., 2012. Critical parameters optimized for accurate phase behavior modeling for heavy *n*-alkanes up to C_{100} using the Peng–Robinson equation of state. Fluid Phase Equilib. 335, 46–59.

Kumar, A., Okuno, R., 2013. Characterization of reservoir fluids using an eos based on perturbation from *n*-alkanes. Fluid Phase Equilib. 358, 250–271.

Kumar, A., Okuno, R., 2014. Reservoir oil characterization for compositional simulation of solvent injection process. Ind. Eng. Chem. Res. 53, 440–455.

Lee, B.I., Kesler, M.G., 1975. A generalized thermodynamic correlation based on three-parameter corresponding states. AIChE J. 21, 510–527.

Li, H., Zheng, S., Yang, D., 2013a. Enhanced swelling effect and viscosity reduction of solvent(s)/CO_2/heavy-oil systems. SPE J. 18, 695–707.

Li, X., Li, H., Yang, D., 2013b. Determination of multiphase boundaries and swelling factors of solvent(s)−CO_2−heavy oil systems at high pressures and elevated temperatures. Energy Fuels 27, 1293–1306.

Lindeloff, N., Mogensen, K., Pedersen, K.S., Tybjerg, P., 2013. Investigation of miscibility behavior of CO_2 rich hydrocarbon systems—with application for gas injection EOR. In: Presented at Annual Technical Conference and Exhibition, New Orleans, LA, USA, 30 Spet.–2Oct. 2013.
McVay, D.A., 1994. Generalization of PVT Properties for Modified Black-Oil Simulation of Volatile and Gas Condensate Reservoirs (Ph.D. Dissertation). Texas A&M University, TX, USA.
Moore, D.C., 1989. Simulation of Gas-Condensate Reservoir Performance Using Schmidt–Wenzel Equation of State (M.Sc. Thesis). Montana College of Mineral Science and Technology, MT, USA.
Negahban, S., Pedersen, K.S., Baisoni, M.A., Sah, P., Azeem, J., 2010. An EoS Model for a middle east reservoir fluid with an extensive EOR PVT data material. In: Presented at Abu Dhabi International Petroleum Exhibition & Conference, Abu Dhabi, UAE, 1–4 Nov. 2010.
Nikitin, E.D., Pavlov, P.A., Popov, A.P., 1997. Vapour–liquid critical temperature and pressure of normal alkanes with from 19 to 36 carbon atoms, napthalene and *m*-terphenyl determined by the pulse-heating technique. Fluid Phase Equilib. 141, 155–164.
Nojabaei, B., Johns, R.T., Chu, L., 2013. Effect of capillary pressure on phase behavior in tight rocks and shales. SPE Reservoir Eval. Eng. 16, 281–289.
PVTsim, 19.2, 2010. Calsep International Consultants, Copenhagen, Denmark.
Pedersen, K.S., Christensen, P.L., 2007. Phase Behavior of Petroleum Reservoir Fluids. CRC Press, Taylor & Francis Group, Boca Raton, FL, USA.
Pedersen, K.S., Thomassen, P., Fredenslund, A.a., 1988. Characterization of gas condensate mixture. In: Presented at the 1988 AIChE Spring National Meeting, New Orleans, LA, March 6–10, 1988.
Pedersen, K.S., Milter, J., Sørensen, H., 2004. Cubic equations of state applied to HT/HP and highly aromatic fluids. SPE J. 9, 186–192.
Peng, D.-Y., Robinson, D.B., 1978. The Characterization of the Heptanes and Heavier Fractions for the GPA Peng–Robinson Programs. GPA Research Report RR-28.
Peng, D.-Y., Robinson, D.B., 1976. A new two-constant equation of state. Ind. Eng. Chem. Fund. 15, 59–64.
Quiñones-Cisneros, S.E., Zéberg-Mikkelsen, C.K., Baylaucq, A., Boned, C., 2004. Viscosity modeling and prediction of reservoir fluids: from natural gas to heavy oils. Int. J. Therm. 25, 1353–1366.
Renner, T.A., Metcalfe, R.S., Yellig Jr., W.F., Spencer, M.F., 1989. Displacement of rich gas condensate by nitrogen: laboratory corefloods and numerical simulations. SPE Reservoir Eng. 4, 52–58.
Reudelhuber, F.O., Hinds, R.F., 1956. A compositional material balance method for prediction of recovery from volatile oil depletion drive reservoirs. Pet. Trans. AIME 210, 19–26.
Riazi, M.R., Daubert, T.E., 1986. Characterization parameter for petroleum fractions. Ind. Eng. Chem. Res. 26, 755–759.
Schulte, A.M., 1980. Compositional variation within a hydrocarbon column due to gravity. In: Presented at SPE Annual Technical Conference and Exhibition, Dallas, September 21–24.
Sharma, G.D., 1990. Development of Effective Gas Solvents Including Carbon Dioxide for the Improved Recovery of West Sak Oil (Report No. DOE/FE/61114-2). University of Alaska Fairbanks, Alaska, USA.
Soave, G., 1972. Equilibrium constants from a modified Redlich–Kwong equation of state. Chem. Eng. Sci. 27, 1197–1203.
Spivak, A., 1971. Mathematical Simulation of Condensate-Gas Reservoirs (Ph.D. Dissertation). University of Texas at Austin, TX, USA.
Subero, C.L., 2009. Numerical Modeling of Nitrogen Injection into Gas Condensate Reservoir (M.Sc. Thesis). West Virginia University, Morgantown, WV, USA.
Søreide, I., 1989. Improved Phase Behavior Predictions of Petroleum Reservoir Fluids from a Cubic Equation of State (Ph.D. Dissertation). The Norwegian Institute of Technology, Norway.
Thodos, G., 1955a. Critical constants of saturated aliphatic hydrocarbons. AIChE, J. 1, 168–173.
Thodos, G., 1955b. Critical constants of unsaturated aliphatic hydrocarbons. AIChE J. 1, 165–168.
Thodos, G., 1956. Critical constants of naphthenic hydrocarbons. AIChE J. 2, 508–513.
Thodos, G., 1957. Critical constants of aromatic hydrocarbons. AIChE J. 3, 428–431.
Tsonopoulos, C., Wilson, G.M., 1983. High-temperature mutual solubilities of hydrocarbons and water. AIChE J. 29, 990–999.
Vogel, J.L., Yarborough, L., 1980. The effect of nitrogen on the phase behavior and physical properties of reservoir fluids. In: Presented at First Joint SPE/DOE Symposium on Enhanced Oil Recovery, April 20–23, 1980. Tulsa, Oklahoma.
Voutsas, E.C., Pappa, G.D., Magoulas, K., Tassios, D.P., 2006. Vapor liquid equilibrium modeling of alkane systems with equation of state: "simplicity versus complexity". Fluid Phase Equilib. 240, 127–139.
Whitaker, C.A., Kim, J.S., 1993. Application of extended equation of state work to optimize the pegasus devonian field unit no. 3 gas cycling operation. In: Presented at SPE Annual Technical Conference and Exhibition, 3–6 October 1993, Houston, Texas.
Whitson, C.H., Belery, P., 1994. Compositional gradients in petroleum reservoirs. In: Paper Presented at the University of Tulsa Centennial Petroleum Engineering Symposium, Tulsa, OK, 29–31 August 1994.
Whitson, C.H., Brulè, M.R., 2000. Phase behaviour. SPE Henry L. Doherty Series, vol. 20. SPE, Richardson, Texas.
Whitson, C.H., Torp, S.B., 1983. Evaluating constant-volume depletion data. J. Pet. Technol. 35, 610–620.
Wijaya, Z., 2006. CO_2 Injection in an Oil Reservoir with Gas Cap (Compositional Simulation Case at Heidrum Field Norway) (M.Sc. Thesis). Norwegian University of Science and Technology, Norway.
Yang, T., Chan, W.-D., Guo, T.M., 1997. Phase behavior of a near-critical fluid mixture. Fluid Phase Equilib. 128, 183–197.
Yarborough, L., 1979. Application of a generalized equation of state to petroleum reservoir fluids. Adv. Chem. 182, 385–439.
Zudkevitch, D., Joffe, J., 1970. Correlation and prediction of vapor–liquid equation with the Redlich–Kwong equation of state. AIChE J. 16, 112–119.